

Accepted Manuscript

Unveiling novel 2-cyclopropyl-3-ethynyl-4-(4-fluorophenyl)quinolines as GPCR ligands via PI3-kinase/PAR-1 antagonism and platelet aggregation valuations; Development of a new class of anticancer drugs with thrombolytic effects

P. Thangarasu, S. Thamarai Selvi, A. Manikandan

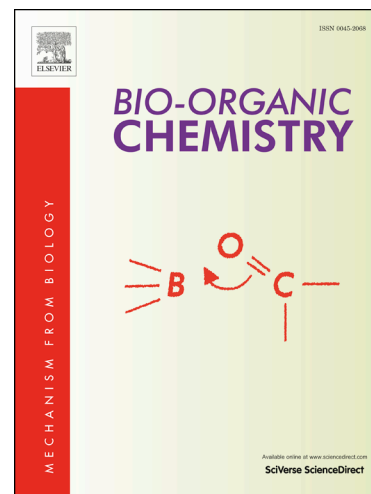
PII: S0045-2068(18)30688-6
DOI: <https://doi.org/10.1016/j.bioorg.2018.09.011>
Reference: YBIOO 2508

To appear in: *Bioorganic Chemistry*

Received Date: 10 July 2018
Revised Date: 26 August 2018
Accepted Date: 7 September 2018

Please cite this article as: P. Thangarasu, S. Thamarai Selvi, A. Manikandan, Unveiling novel 2-cyclopropyl-3-ethynyl-4-(4-fluorophenyl)quinolines as GPCR ligands via PI3-kinase/PAR-1 antagonism and platelet aggregation valuations; Development of a new class of anticancer drugs with thrombolytic effects, *Bioorganic Chemistry* (2018), doi: <https://doi.org/10.1016/j.bioorg.2018.09.011>

This is a PDF file of an unedited manuscript that has been accepted for publication. As a service to our customers we are providing this early version of the manuscript. The manuscript will undergo copyediting, typesetting, and review of the resulting proof before it is published in its final form. Please note that during the production process errors may be discovered which could affect the content, and all legal disclaimers that apply to the journal pertain.



Unveiling novel 2-cyclopropyl-3-ethynyl-4-(4-fluorophenyl)quinolines as GPCR ligands via PI3-kinase/PAR-1 antagonism and platelet aggregation valuations; Development of a new class of anticancer drugs with thrombolytic effects

Thangarasu P^a, Thamarai Selvi S^{c,*} and Manikandan A^{b,**}

^aResearch and Development Centre, Bharathiar University, Coimbatore - 641046, India.

^bPG and Research Department of Chemistry, Government Arts College, Coimbatore- 641018, Tamil Nadu, India.

^cDepartment of Biotechnology, School of Bio-Sciences and Technology, VIT University, Vellore-632014, India.

Corresponding authors: * thamaraimohan@gmail.com; ** mailtomicromani@gmail.com

Abstract

In the present study, novel 2-cyclopropyl-3-ethynyl-4-(4-fluorophenyl) quinolines (**4a-l**) were recognized and evaluated as G-Protein Coupled Receptor (GPCR) ligands through molecular evaluations. Thrombin mediates adhesion of mast cell, a type of cell abundantly found in connective tissue and releasing histamine and other substances during inflammatory and allergic reactions, through phosphoinositol 3-kinase pathway. With this background, as preliminary, **4a-l** are resolute to be potential leads, designated from their effective phosphoinositol 3-kinase (PI3-Kinase) inhibition potentials, best-docked scores, comparative ligand efficiency, and significant structural attributes evaluated by *ab initio* simulations. Since thrombin is one of the main reason for various cancer invasion in association with PI3Kinase, a thrombolytic potential of the compounds also analyzed. The experimental *in vitro* studies confirmed the significant enhancement as PI3Kinase inhibitors and appreciable enhancement in MTT assay of breast and skin cancer cell lines. Significantly, acetophenone substituent in the quinoline scaffold could be coherent to note the significant binding affinity to all the evaluated drug targets.

Keywords: Anti-inflammatory; Anticancer; GPCR Ligands; Molecular docking; MTT assay; PAR1; PI3Kinase; Quinolines; XRD.

Introduction:

Due to the presence of highly expressible affinity to various proteins, which are involving in a disease's instigation and development, makes quinoline and their derivatives are acting as an important class of compounds in new drug design and development. Quinoline and its fused heterocyclic compounds are biologically as well as medicinally significant functional entities [1,2]. So far, a wide range of quinoline-based derivatives were targeted as anticancer [3], antibiotic [4], anti HIV [5], anti-mycobacterial [6], antimalarial [7], anti-inflammatory [8], antihypertensive [9], antibacterial [10] and cardiovascular [11] agents. Present work deals about the preparation of novel 2-cyclopropyl-3-ethynyl-4-(4-fluorophenyl) quinoline and its related compounds to evaluate them as effective G-Protein Coupled Receptor (GPCR) ligands through Protease-Activated Receptor-1 (PAR-1) expressions. To achieve the targeted quinoline derivatives, we have approached two methods namely Ohira-Bestmann synthesis [12, 13] and Sonogashira coupling methods [14, 15].

Comparatively, according to our experimental experience, Ohira-Bestmann synthesis was reliable. For this reason, we opt Ohira-Bestmann synthesis and followed by Sonogashira Coupling methods to achieve novel 2-cyclopropyl-3-ethynyl-4-(4-fluorophenyl)quinoline derivatives (Fig. 1) **4a-1** and the method was most reliable and economical. A prediction based preliminary screening against the most potent bioactivity possessed by **4a-1** executed. Open bioactivity prediction online-sites like Molinspiration and PASSonline used for the prediction. Molinspiration, a proficient system for the calculation of drug-likeness score, allows predicting GPCR ligands, ion channel modulators, kinase inhibitors, nuclear receptor ligands, protease inhibitors and other enzyme targets (<http://www.molinspiration.com/cgi-bin/properties>).

PASSonline selecting the prospective compounds for High-throughput screening (<http://www.pharmaexpert.ru/PASSonline/predict.php>).

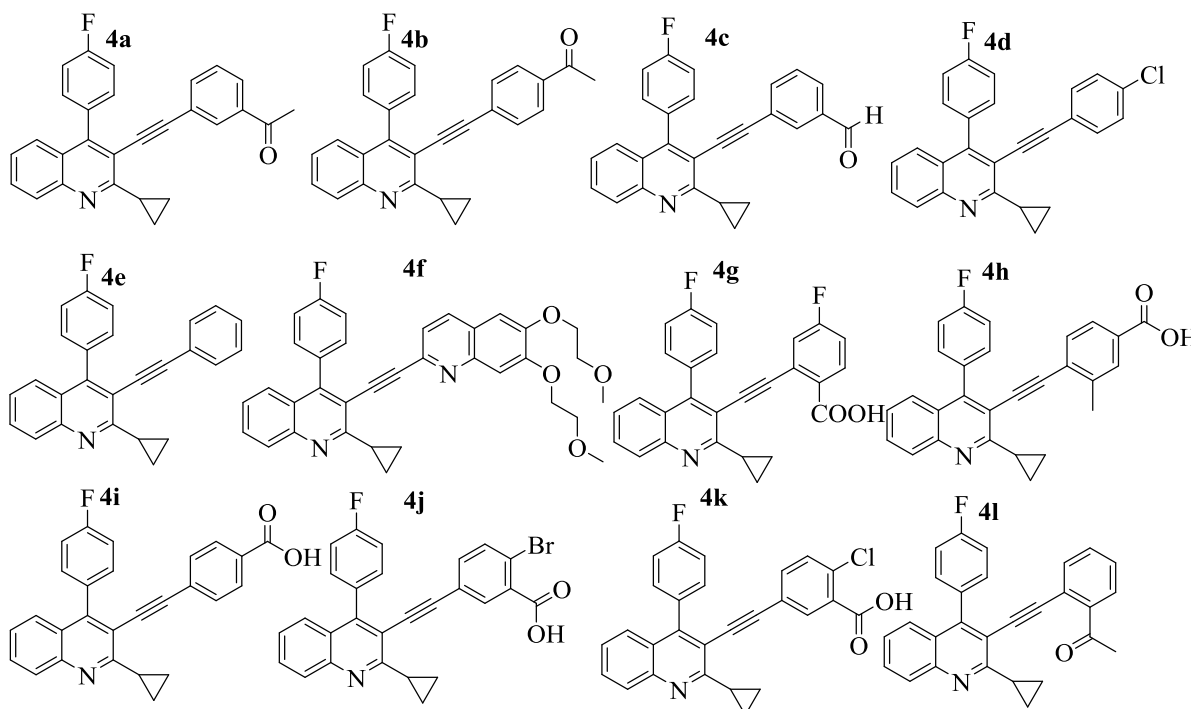


Figure 1. 2-cyclopropyl-3-ethynyl-4-(4-fluorophenyl) quinoline derivatives

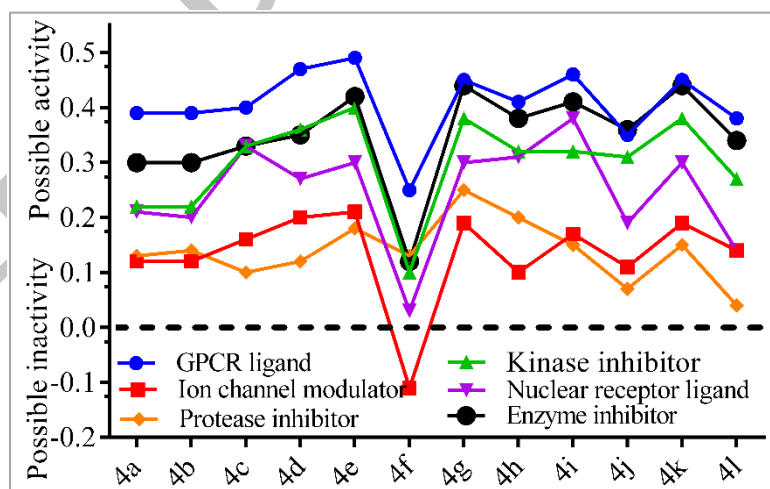


Figure 2. Bioactivity prediction data of 2-cyclopropyl-3-ethynyl-4-(4-fluorophenyl)quinolines (4a-l)

Fig. 2 depicts the vicissitudes of 4a-l towards all the above-mentioned categories. In the first look, GPCR ligand potency (data set in blue) of all compounds (4a-l) and impotency of 4f towards all activity was recognized. The dataset (Fig. 2) in black are the obtained possible

enzyme inhibition potential values of **4a-1**. This reveals the possible antagonism effects of **4a-1** against any enzyme that are highly responsible for numerous diseases and their developments. The derived kinase inhibition values of **4a-1** prescribed to execute a selective kinase mechanism based biological activity where the GPCR playing a vital role. Protease-activated receptor 1 (PAR1) is an unusual GPCR that interacts with multiple G protein subfamilies ($G_{q/11}$, $G_{i/o}$, and $G_{12/13}$) and their linked signaling pathways are regulating a broad range of pathophysiological processes [16]. Most importantly, the coagulation and fibrinolytic systems contribute to malignancy by increasing angiogenesis, tumor growth, tumor invasion, and tumor metastasis [17]. Tissue factor (TF) is the cell surface receptor for coagulation factor VII/VIIa (FVII/VIIa). TF is expressed on various cell types and its expression is up-regulated by oncogenic transformation, conferring a procoagulant phenotype to cancer cells [18,19].

Methods and Materials

All organic chemicals and solvents procured from Sigma-Aldrich, Merck, and Spectrochem. Solvents (commercial) and chemicals used as received without doing any further purification. For thin-layer chromatography (TLC) analysis, Merck pre-coated plates (silica gel 60 F254) used and spots visualized under UV light. Merck silica gel 60 (230-400 mesh) was used for flash column chromatography and the eluting solvents are indicated in the procedures. Melting point (mp) determinations performed using an OptiMelt automated melting point system and are uncorrected. ^1H NMR (400 MHz) and ^{13}C NMR (100 MHz) spectra were recorded on Bruker-400 MHz instrument. Mass spectra recorded on Agilent ion trap MS and Infrared (IR) spectra recorded on Perkin Elmer FT-IR spectrometer. HPLC analysis of all the compounds carried out on an Agilent 1260 series HPLC with an Agilent Extend-C18 column.

Synthesis of title compounds, quinoline derivatives (4a-l)

In the present study, the final quinoline derivatives (**4a-l**) were achieved from 2-cyclopropyl-3-ethynyl-4-(4-fluorophenyl)quinoline (**3**). To achieve compound **3**, we have used Ohira-Bestmann synthesis, a single step process. Dimethyl-2-oxopropylphosphonate 6.84 g (0.12 mol), was added to the mixture of potassium carbonate 21.31 g (0.45 mol) and 1H-imidazole-1-sulfonyl azide hydrochloride 9.35 g (0.13 mol) in acetonitrile (20 ml). The mass was stirred for 2 hr at 25 °C. Then added 10 g of 2-cyclopropyl-4-(4-fluorophenyl)quinoline-3-carbaldehyde (0.10 mol) in methanol (10 ml) to the above suspension, the mass was stirred for 15 hours at 25 °C. The reaction was completed as indicated by TLC and the mixture was filtered, washed the bed with ethyl acetate 50 ml and concentrated the filtrate at 50-55 °C under vacuum. 50 ml of water was added, the product was extracted in ethyl acetate (4* 50 ml), and the combined organic layers were washed with brine (2* 50 ml), dried with sodium sulfate, filtered and concentrated at 50-55 °C under vacuum. Later stripped up with 10 ml of isopropyl alcohol. Then IPA 30.0 ml added and the temperature raised to 50-55 °C. The mass stirred at 55-60 °C for 30 mins, the temperature reduced to 25-30 °C. The mass was stirred again for another 2-3 hours at 25-30 °C.

The mass was filtered and washed the wet cake with 5 ml of IPA, then dried to get pure solid (5.91 g, 60 %), 2-cyclopropyl-3-ethynyl-4-(4-fluorophenyl)quinoline (**3**). Melting point: 115-117 °C. IR (KBr): 3306, 3066, 3009, 2082, 1445, 1224 cm^{-1} . ^1H NMR: NMR (400 MHz, DMSO-d_6) δ ppm: 1.13-1.15 (d, 2H, J=8.0), 1.20 (s, 2H), 2.86 (m, 1H), 4.49 (s, 1H), 7.36-7.51(m, 6H), 7.70-7.74 (t, 1H, J= 8), 7.89-7.91 (d, 1H, J=8). ^{13}C NMR (100 MHz, DMSO-d_6) δ ppm: 11.10, 15.28, 79.99, 89.78, 115.04, 115.29, 115.54, 124.46, 125.66, 126.31, 130.33, 131.75, 132.35, 146.13, 149.77, 160.88, 162.46, 163.32. MS (EI, m/z): 288.1 (M+1). HPLC

purity: 96.35 %. Anal calcd for C₂₀H₁₄FN: C, 83.60; H, 4.91; F 6.61; N, 4.87 %; Found: C, 83.61; H, 4.90; F, 6.60; N, 4.88 %.

General procedure for the preparation of derivatives of 2-cyclopropyl-3-ethynyl-4-(4-fluorophenyl) quinoline derivatives (4a-l) using Sonogashira Coupling: To a solution of 0.5 g compound 3 (0.10 mol) in 3 ml DMF, 3.3 mg (0.01 mol) of copper iodide, 0.57 g cesium carbonate (0.1 mol), 20 mg (0.01 mol) Tetrakis (triphenylphosphine) palladium(0) was added under nitrogen atmosphere. Then aryl halide (4-12) 0.11 mol was added under nitrogen atm, the mass was stirred for 8 hrs at 75 °C under nitrogen atm. Reaction was completed as indicated by TLC and the reaction mass was filtered through cellite bed, washed the bed with ethyl acetate (10 ml). The product layer (Ethyl acetate layer) was then washed with water 10.0 ml, sodium bisulphite 10 ml followed by saturated sodium chloride solution (5.0 ml) and dried over (Na₂SO₄). The solvent was distilled off and the resulting product was purified by column chromatography using ethyl acetate and n-hexane to get the pure product (**4a-l**). Yield observed was around 85-90 % for all the derivatives.

1-(3-((2-cyclopropyl-4-(4-fluorophenyl)quinolin-3-yl)ethynyl)phenyl)ethanone (4a): The aryl halide 3- Bromo aceto phenone was used to prepare **4a**. Melting point: 143.4-145.2 °C. IR (KBr): 3063, 2997, 2212, 1427, 1384, 1681, 1512, 1222, 812 cm⁻¹. ¹H NMR: NMR (400 MHz, DMSO-d₆) δ ppm: 1.17-1.19 (d, 2H, J= 7.2), 1.24 (s, 2H), 2.56 (s, 3H), 2.94-2.95 (m, 1H), 7.44-7.52 (m, 6H), 7.54-7.60 (m, 2H), 7.69-7.72 (m, 2H), 7.89-7.93 (m, 2H). ¹³C NMR (100 MHz, DMSO-d₆) δ ppm: 11.19, 15.59, 26.60, 54.83, 87.27, 97.03, 115.15, 115.36, 122.44, 124.42, 125.62, 126.30, 128.43, 128.58, 129.21, 130.29, 130.48, 131.94, 132.02, 132.42, 135.04, 137.03, 146.33, 149.42, 160.94, 161.93, 163.38, 196.98. MS (EI, m/z): 406.3 (M+1). HPLC purity: 99.80 %. Anal calcd for C₂₈H₂₀FNO: C, 82.94; H, 4.97; F, 4.89; N, 3.45, O, 3.95 %; Found:

C,82.95; H, 4.99; F, 4.87; N, 3.47, O, 3.96 %; HRMS Calculated [M⁺] m/z 405.4724, Found 405.4724.

1-(4-((2-cyclopropyl-4-(4-fluorophenyl)quinolin-3-yl)ethynyl)phenyl)ethanone (4b): The aryl halide 4-Bromo aceto phenone was used for the preparation of **4b**. Melting point: 165.1-166.5 °C. IR (KBr): 3068, 3001, 2210, 1677, 1438, 1356, 1222, 834 cm⁻¹. ¹H NMR: NMR (400 MHz, DMSO-d₆) δ ppm: 1.18-1.20 (d, 2H, J= 8), 1.25 (s, 2H), 2.57 (s, 3H), 2.93-2.94 (m, 1H), 7.37-7.39 (d, 2H, J=8), 7.42-7.49 (m, 4H), 7.51-7.61 (m, 2H), 7.72-7.75 (m, 1H), 7.88-7.98 (m, 3H). ¹³C NMR (100 MHz, DMSO-d₆) δ ppm: 11.20, 15.65, 26.72, 30.65, 89.43, 97.13, 115.21, 115.43, 124.44, 125.75, 126.44, 128.47, 128.63, 130.51, 131.18, 131.95, 132.04, 146.45, 149.63, 162.04, 197.17. MS (EI, m/z): 406.5 (M+1). HPLC purity: 99.66 %. Anal calcd for C₂₈H₂₀FNO: C,82.94; H, 4.97; F, 4.89; N, 3.45, O, 3.95 %; Found: C,82.92; H, 4.95; F, 4.89; N, 3.47, O, 3.97 %; HRMS Calculated [M⁺] m/z 405.4724, Found 405.4725.

3-((2-cyclopropyl-4-(4-fluorophenyl)quinolin-3-yl)ethynyl)benzaldehyde (4c): Aryl halide 3-Bromo benzaldehyde was used for the preparation of **4c**. Melting point: 117.6-119.6 °C. IR (KBr): 3057, 3003, 2215, 1697, 1435, 1383, 1223 cm⁻¹. ¹H NMR: NMR (400 MHz, DMSO-d₆) δ ppm: 1.17-1.19 (d, 2H, J= 8), 1.24 (s, 2H), 2.95 (s, 3H), 7.36-7.45 (m, 4H), 7.51-7.53 (d, 1H, J=8.0), 7.56-7.62 (m, 3H), 7.70-7.73 (m, 1H), 7.87-7.91 (m, 2H), 9.97 (s, 1H). ¹³C NMR (100 MHz, DMSO-d₆) δ ppm: 11.15, 15.60, 87.61, 96.57, 115.17, 115.25, 115.39, 122.89, 124.40, 125.65, 126.32, 128.59, 129.57, 129.65, 130.33, 130.71, 131.61, 131.91, 131.99, 132.34, 136.35, 146.33, 146.36, 149.36, 160.95, 162.00, 163.31, 192.32. MS (EI, m/z): 392.2 (M+1). HPLC purity: 90.80 %. Anal calcd for C₂₇H₁₈FNO: C,82.85; H, 4.63; F, 4.85; N, 3.58; O, 4.09 %; Found: : C,82.87; H, 4.65; F, 4.82; N, 3.60, O, 4.07 %; HRMS Calculated [M⁺] m/z 391.4454, Found 391.4456.

3-((4-chlorophenyl)ethynyl)-2-cyclopropyl-4-(4-fluorophenyl)quinoline (4d): Aryl halide 4-Bromo chloro benzene was used for the preparation of **4d**. Melting point: 151.3-153.2 °C. IR (KBr): 3042, 3008, 2210, 1439, 1416, 1225, 1013 cm^{-1} . ^1H NMR: NMR (400 MHz, CDCl_3) δ ppm: 1.17-1.19 (d, 2H, J=8), 1.23-1.24(d, 2H, J=4), 2.91-2.95 (m, 1H), 7.27-7.29 (d, 2H, J=8), 7.43-7.50 (m, 6H), 7.56-7.60 (m, 2H), 7.71-7.75 (m, 1H), 7.90-7.92 (d, 1H, J=8). ^{13}C NMR (100 MHz, CDCl_3) δ ppm: 10.80, 15.97, 87.77, 97.07, 115.09, 115.31, 116.29, 121.50, 125.13, 125.82, 125.87, 128.73, 129.11, 129.74, 131.78, 131.86, 132.45, 133.0, 134.54, 147.01, 149.25, 162.59, 163.95. MS (EI, m/z): 398.3 (M+2). HPLC purity: 94.52 %. Anal calcd for $\text{C}_{26}\text{H}_{17}\text{ClFN}$: C, 78.49; H, 4.31; Cl 8.91; F, 4.78; N, 3.52 %; Found: C, 78.48; H, 4.32; Cl 8.93; F, 4.77; N, 3.51 %; HRMS Calculated [M+] m/z 397.8774, Found 397.8774.

2-cyclopropyl-4-(4-fluoro phenyl)-3-(phenyl ethynyl) quinoline (4e): The aryl halide, Iodo benzene was used for the preparation of **4e**. Melting point: 101.2-103.0 °C. IR (KBr): 3059, 3005, 2205, 1600, 1487, 1442, 1218, 1093, 1024 cm^{-1} . ^1H NMR: NMR (400 MHz, CDCl_3) δ ppm: 1.16-1.18 (d, 2H, J= 8), 1.24 (s, 2H), 2.94 (m, 1H), 7.25-7.26 (d, 2H, J=4), 7.36-7.44 (m, 3H), 7.54-7.57 (m, 3H), 7.63-7.82 (m, 2H), 7.85-7.90 (m, 1H), 8.69-8.72(d, 2H, J=12). ^{13}C NMR (100 MHz, CDCl_3) δ ppm: 11.00, 15.52, 86.35, 97.92, 115.06, 115.27, 115.64, 121.96, 124.43, 125.53, 126.18, 128.53, 128.63, 128.92, 129.13, 130.05, 130.62, 130.92, 131.85, 131.93, 132.06, 132.44, 146.19, 148.84, 161.94, 163.30. MS (EI, m/z): 364.4 (M+1). HPLC purity: 94.85 %. Anal calcd for $\text{C}_{26}\text{H}_{18}\text{FN}$: C, 85.93; H, 4.99; F, 5.23; N, 3.85 %; Found: C, 85.95; H, 4.98; F, 5.24; N, 3.86 %; HRMS Calculated [M+] m/z 363.4354, Found 363.4353.

3-((6,7-bis(2-methoxyethoxy)quinolin-2-yl)ethynyl)-2-cyclopropyl-4-(4-fluorophenyl)

quinoline (4f): The aryl halide 2-chloro-6,7-bis(2-methoxyethoxy)quinoline was used for the preparation of **4f**: Melting point: 133.8-135.6 °C. IR (KBr): 3059, 2983, 2200, 1443, 1180 cm^{-1} .

^1H NMR: NMR (400 MHz, CDCl_3) δ ppm: 1.19-1.22 (m, 2H), 1.43-1.44(m, 2H), 3.04-3.08 (m, 1H), 3.51 (s, 6H), 3.86-3.90 (m, 4H), 4.06-4.08 (t, 2H, J=8), 4.31-4.33 (t, 2H, J=8), 7.02 (s, 1H), 7.23-7.28 (m, 3H), 7.39-7.43 (m, 1H), 7.53-7.58 (m, 3H), 7.68-7.72 (m, 1H), 8.00-8.02 (d, 1H, J=8), 9.11 (s, 1H). ^{13}C NMR (100 MHz, CDCl_3) δ ppm: 11.29, 16.07, 59.32, 68.62, 68.84, 70.33, 70.53, 93.73, 94.29, 104.86, 107.57, 114.75, 115.44, 115.65, 121.25, 124.86, 126.05, 130.47, 131.75, 131.83, 132.47, 147.53, 148.34, 150.23, 150.59, 153.75, 156.10, 161.56, 163.25, 164.03. MS (EI, m/z): 564.3 (M+1). HPLC purity: 97.37 %. Anal calcd for $\text{C}_{35}\text{H}_{31}\text{FN}_2\text{O}_4$: C, 74.72; H, 5.55; F, 3.38; N, 4.98; O, 11.37 %; Found: C, 74.74; H, 5.55; F, 3.6; N, 4.99; O, 11.39 %; HRMS Calculated [M+] m/z 562.6414, Found 562.6414.

2-((2-cyclopropyl-4-(4-fluorophenyl)quinolin-3-yl)ethynyl)-4-fluorobenzoic acid (4g): Aryl halide used for the preparation of compound **3g** is 2-Bromo 4-fluoro benzoic acid. Melting point: 181.2-182.7 °C. IR (KBr): 3435, 3017, 2853, 1728, 1654, 1515, 1246 cm^{-1} . ^1H NMR: NMR (400 MHz, CDCl_3) δ ppm: 1.18-1.19 (m, 2H), 1.20 (s, 2H), 2.95-3.01 (m, 1H), 7.45-7.51 (m, 4H), 7.58-7.62 (m, 2H), 7.62-7.70 (m, 2H), 7.73-7.76 (m, 1H), 7.91-7.93 (d, 1H, J=8), 8.00 (s, 1H), 13.59 (s, 1H, D_2O exchangeable). ^{13}C NMR (100 MHz, CDCl_3) δ ppm: 11.31, 15.62, 88.73, 95.42, 115.02, 115.17, 115.39, 121.81, 124.37, 125.70, 126.38, 128.61, 130.47, 131.97, 132.31, 133.38, 136.91, 146.48, 149.87, 162.06, 165.07. MS (EI, m/z): 426.40 (M+1). HPLC purity: 95.57 %. Anal calcd for $\text{C}_{27}\text{H}_{17}\text{F}_2\text{NO}_2$: C, 76.23; H, 4.03; F, 8.93; N, 3.29; O, 7.52 %; Found: C, 76.24; H, 4.02; F, 8.93; N, 3.30; O, 7.53 %; HRMS Calculated [M+] m/z 425.4348, Found 425.4349.

4-((2-cyclopropyl-4-(4-fluorophenyl)quinolin-3-yl)ethynyl)-3-methylbenzoic acid (4h): The aryl halide 4-Bromo 3-methyl benzoic acid was used for the preparation of **4h**. Melting point: 202.1-204.5 °C. IR (KBr): 3433, 3070, 3006, 2201, 1692, 1653, 1488, 1263, 1224 cm^{-1} . ^1H NMR:

NMR (400 MHz, DMSO- d_6) δ ppm: 1.17-1.19 (d, 2H, J=8), 1.25 (s, 2H), 2.07 (s, 3H), 2.94-2.95 (m, 1H), 7.39-7.48 (m, 5H), 7.53-7.56 (m, 2H), 7.61-7.64 (m, 2H), 7.66-7.79 (m, 1H), 7.90-7.92 (d, 1H, J=8), 13.01 (s, 1H, D₂O exchangeable). ¹³C NMR (100 MHz, DMSO- d_6) δ ppm: 10.90, 15.66, 19.51, 92.60, 96.13, 115.35, 115.57, 124.60, 125.67, 126.11, 126.35, 126.63, 128.56, 130.19, 130.35, 130.66, 131.65, 132.61, 139.34, 146.26, 149.23, 161.00, 161.99, 166.67. HPLC purity: 90.74 %. MS (EI, m/z): 564.3 (M+1). Anal calcd for C₂₈H₂₀FNO₂: C, 79.79; H, 4.78; F, 4.51; N, 3.32; O, 7.59 %; Found: C, 79.80; H, 4.77; F, 4.53; N, 3.30; O, 7.58 %; HRMS Calculated [M+] m/z 421.4714, Found 421.4716.

4-((2-cyclopropyl-4-(4-fluorophenyl)quinolin-3-yl)ethynyl)benzoic acid (4i): Aryl halide 4-Bromo benzoic acid was used for the preparation of compound **4i**. Melting point: 196.2-198.1 °C. IR (KBr): 3448, 3056, 3004, 2204, 1680, 1420, 1224 cm⁻¹. ¹H NMR: NMR (400 MHz, DMSO- d_6) δ ppm: 1.18-1.24 (d, 4H), 2.3 (m, 1H), 7.37-7.46 (m, 8H), 7.57-7.71 (m, 1H), 7.91 (m, 3H), 13.13 (s, 1H, D₂O exchangeable). ¹³C NMR (100 MHz, DMSO- d_6) δ ppm: 11.05, 15.59, 89.0, 97.07, 115.14, 115.23, 115.35, 124.39, 124.65, 126.17, 126.31, 128.58, 129.47, 130.34, 130.73, 131.03, 131.87, 131.95, 132.27, 146.40, 149.39, 160.93, 162.01, 166.51. MS (EI, m/z): 408.5 (M+1). HPLC purity: 94.93 %. Anal calcd for C₂₇H₁₇FNO₂: C, 79.59; H, 4.45; F, 4.66; N, 3.44; O, 7.85 %; Found: C, 79.58; H, 4.46; F, 4.68; N, 3.45; O, 7.86 %; HRMS Calculated [M+] m/z 407.4444, Found 407.4445.

2-bromo-6-((2-cyclopropyl-4-(4-fluorophenyl)quinolin-3-yl)ethynyl)benzoic acid (4j): Aryl halide 2-Bromo 5-iodo benzoic acid was used for the preparation of **4j**. Melting point: 210.2-211.8 °C. IR (KBr): 3449, 3061, 3004, 2204, 1676, 1420, 1227 cm⁻¹. ¹H NMR: NMR (400 MHz, DMSO- d_6) δ ppm: 1.16-1.20 (m, 2H), 1.24 (s, 2H), 2.95-3.01 (m, 1H), 7.45-7.51 (m, 4H), 7.58-7.62 (m, 2H), 7.67-7.70 (m, 2H), 7.73-7.76 (t, 1H, J=6.4), 7.91-7.93 (d, 1H, J=8.4), 8.00 (s, 1H),

13.18 (s, 1H, D₂O exchangeable). ¹³C NMR (100 MHz, DMSO-d₆) δ ppm: 11.31, 15.62, 88.73, 95.42, 115.02, 115.17, 115.39, 121.81, 124.37, 125.76, 128.61, 130.47, 132.97, 132.31, 133.38, 136.91, 146.84, 149.87, 162.06, 165.07. MS (EI, m/z): 486.6 (M+2). HPLC purity: 94.90 %. Anal calcd for C₂₇H₁₇BrFNO₂: C, 66.68; H, 3.52; Br, 16.43; F, 3.91; N 2.88; O, 6.58 %; Found: C, 66.70; H, 3.54; Br, 16.44; F, 3.90; N, 2.89; O, 6.59 %; HRMS Calculated [M+] m/z 486.3404, Found 486.3405.

2-chloro-5-((2-cyclopropyl-4-(4-fluorophenyl)quinolin-3-yl)ethynyl) benzoic acid (4k): The aryl halide 5-Bromo 2-chloro benzoic acid was used for the preparation of **4k**. Melting point: 181.2-182.7 °C. IR (KBr): 3431, 3075, 3012, 1725, 1556, 1512, 1419, 1193, 1171, 1041 cm⁻¹. ¹H NMR: NMR (400 MHz, CDCl₃) δ ppm: 1.18-1.20 (d, 2H, J=8), 1.24 (s, 2H), 2.89-2.95 (m, 1H), 7.36-7.38 (d, 2H, J=8), 7.43- 7.51 (m, 4H), 7.57-7.61 (m, 4H), 7.73-7.76 (m, 1H), 7.91-7.93 (d, 1H, J=8), 13.65 (s, 1H, D₂O exchangeable). ¹³C NMR (100 MHz, CDCl₃) δ ppm: 11.19, 15.60, 59.68, 88.21, 95.89, 115.17, 115.37, 121.02, 124.40, 125.67, 126.37, 128.59, 130.41, 131.25, 131.93, 132.01, 132.30, 132.91, 134.27, 146.39, 149.53, 160.95, 161.99, 163.40, 165.72. MS (EI, m/z): 442.3 (M+1). HPLC purity: 97.41 %. Anal calcd for C₃₅H₃₁FN₂O₄: C, 74.72; H, 5.55; F, 3.38; N, 4.98; O, 11.37 %; Found: C, 74.74; H, 5.56; F, 3.39; N, 4.97; O, 11.35 %; HRMS Calculated [M+] m/z 441.8864, Found 441.8866.

1-(2-((2-cyclopropyl-4-(4-fluorophenyl)quinolin-3-yl)ethynyl)phenyl)ethanone (4l): Aryl halide 2-Bromo aceto phenone was used for the preparation of **4l**. Melting point: 177.5-178.5 °C. IR (KBr): 3067, 3004, 2204, 1767, 1438, 1384, 1221 cm⁻¹. ¹H NMR: NMR (400 MHz, DMSO-d₆) δ ppm: 1.21-1.29 (m, 4H), 3.21 (m, 1H), 7.22-7.24 (d, 1H, J=8), 7.47-7.54 (m, 5H), 7.56-7.60 (m, 3H), 7.76-7.77 (m, 1H), 7.85-7.87 (d, 1H, J=8), 7.94-7.96 (d, 1H, J=8). ¹³C NMR (100 MHz, DMSO-d₆) δ ppm: 10.90, 11.09, 14.71, 15.43, 28.82, 90.72, 96.93, 115.17, 115.39, 115.57,

115.75, 120.00, 124.48, 125.63, 126.26, 127.24, 128.55, 128.87, 129.07, 130.26, 131.57, 131.92, 132.00, 132.19, 132.41, 133.70, 139.44, 146.31, 149.17, 160.94, 162.50, 163.38, 198.80. MS (EI, m/z): 406.2 (M+1). HPLC purity: 90.08 %. Anal calcd for C₂₈H₂₀FNO: C, 82.94; H, 4.97; F, 4.89; N, 3.45, O, 3.95 %; Found: C, 82.93; H, 4.90; F, 4.88; N, 3.46, O, 3.94 %; HRMS Calculated [M+] m/z 405.4724, Found 405.4726.

Single crystal ORTEP and DFT studies

Single-crystal X-ray diffraction data were collected using Oxford XCalibur, Gemini diffractometer equipped with EOS CCD detector at 25 °C with MoK α radiation ($\lambda = 0.71073$ Å). The data reduced using CrysAlisPro Software and multi-scan absorption correction applied using multi Ψ -scans. The structural model was refined by full-matrix least squares against F^2 using the SHELXL-97 software. Non-hydrogen atoms were refined with anisotropic thermal parameters. All hydrogen atoms assigned fixed Uiso values, equal to 1.2Ueq of the parent atom for ring hydrogen atoms. Crystallographic data for the structure had deposited with the Cambridge Crystallographic Data Centre (CCDC No.:1542607). Molecular graphics done by ORTEP 3 and that of molecular packing with MERCURY [20]. The quantum chemical calculations performed by DFT at B3LYP/LAN 12dz level of basis set, using the Gaussian 09 program package [21]. Optimized parameters such as bond lengths and bond angles measured using a molecular visualization package CHEMCRAFT [22].

Interrelation of thrombin, PARs and PI3 Kinase and the experiment details of PI3Kinase inhibition activity assay

Thrombin intercedes most of its cellular activities over the triggering of a series of G protein-coupled receptors (GPCRs). These GPCRs are nothing but the protease-activated receptors

(PARs). These PARs are mainly expressed in the exterior region of almost all cell types [23,24]. In such a condition, Phosphoinositide 3-kinases (PI3 Kinases), an intracellular signal transducer enzymes, play a vital role in regulating functional responses in a variety of hemopoietic cells, including neutrophils, monocytes, mast cells, eosinophils, and B- and T-cells [25]. In a recent research, thrombin found as the mediator of mast cell adhesion through the activation of phosphoinositol 3-kinase pathways [26]. Thus, the small molecules that were inhibiting PI3 Kinases could be the effective anticancer medications. In the present study, the inhibitory potentials of the quinoline derivatives (**4a-1**) were assessed using Glutathione-coated 96 well plate assay as we reported earlier [27-30]. The kinase and the quinoline compounds **4a-1** were pre-incubated for 10-15 minutes before adding PIP2 (Phosphatidylinositol biphosphate) substrate. 5 μ L of 5X Kinase reaction buffer was added followed by the addition of 5 μ L/well of PIP2 substrate to each well. Double distilled water was added each well to make up the final volume as 25 μ L/well. Further, the reaction mixture incubated at 37 $^{\circ}$ C for 60 minutes. The absorbance read at 450 nm. The relative % to b-PIP3 was calculated using the following formula,

$$\% \text{ inhibition} = \frac{\text{OD of samples (buffer, kinase \& inhibitors)}}{\text{OD of B-PIP3 average}} \times 100$$

Molecular docking studies

Based on the bioactivity predictions (Fig. 2), the efficiency of the compounds towards GPCR ligand and kinase inhibition was initially assessed through molecular docking. Both are highly involved in many cancer invasions through thrombin. Protease-activated receptor 1 (PAR1) is the typical adherent element of a family of G-protein-coupled receptors that facilitate cellular activities to thrombin and associated proteases. To get insight into the mode of binding to GPCR and Phosphoinositide Kinase (PI3Kinase), the ligands (**4a-1**) were docked into the active site of

the X-ray crystallography structures of GPCR and PI3Kinase. The PDB structure of PAR1, PDB ID: 3vw7 (<https://www.rcsb.org/structure/3VW7>) and PI3Kinase, PDB ID: 3T8M (<https://www.rcsb.org/structure/3T8M>). We achieved the docking process by referring our previous reports with necessary changes that were needed for the present study [31,32].

***In-vitro* thrombolytic study**

The best PI3Kinase inhibitors of this study compound **4a**, **4b**, **4g**, and **4j** were analyzed for their thrombolytic effects. The thrombolytic study carried out as reported earlier with necessary modifications [32]. The coagulation and fibrinolytic systems contribute to malignancy by increasing angiogenesis, tumor growth, tumor invasion, and tumor metastasis [33]. The mechanism by which coagulation proteases exert their tumor-enhancing effects is, in part, via activation of protease-activated receptor PAR-1 and PAR-2 [34, 35]. Protease-activated receptors (PAR) mediated crosstalk among coagulation and fibrinolysis was studied by Troy *et al.* 2010 [33]. PARs belong to the GPCR family that proteolytically triggered by various proteases. Stimulation of fibrinolysis by plasmin through the infusion of tissue plasminogen activator facilitating the thrombolysis.

A stock suspension of streptokinase was prepared (100 μ L (30,000 I.U)) and used for *in vitro* thrombolysis. 5 ml blood was collected from each healthy volunteers from different age groups (human, n = 4). The blood was transferred (750 μ L) to each of Eppendorf tubes to form clots by incubating at room temperature for 1 h. Serum was aspirated by not disturbing the clot. The weight of blood containing Eppendorf tubes measured before and after the clot formation even after the removal of serum. After administering the compounds **4a**, **4b**, **4g** and **4j** in various concentrations, tubes were incubated at room temperature for 120 minutes and the fluid

formation was observed. Tubes yet again weighed after removing fluid that has formed to recognize the variation in weight after the clot distraction. The variations in weight measured before and after clot lysis stated as a percentage. Streptokinase (thrombolytic) and Millipore water (non-thrombolytic) served as standard and control, respectively.

Platelet aggregation and adhesion assay

Platelet aggregation and adhesion assay evaluated for the best PI3Kinase inhibitor of this study (i.e. compound **4a**). Platelet aggregation was determined by a turbidimetric method with a dual channel aggregometer (Model 591/592, Chrono-Log Corp., Havertown, PA, USA) [36]. Shortly, 250 μ L of platelet-rich plasma (PRP) taken along with various concentrations of quinoline derivatives (25-250 μ g/mL) in glass cuvette and pre-incubated for 3 min at room temperature. The aggregation was commenced by adding collagen (1.5 μ g/mL)/ADP (5 μ M)/epinephrine (5 μ M) and constantly stirred for 10 min (1200 rpm) [37]. Platelet adhesion assay carried out according to previous reports [38, 39]. In a 96-well microtiter plate, the collagen immobilized by adding 25 μ g of collagen type I in 250 μ L of 10 mM (pH 7.4) phosphate buffered saline (PBS) to each well and incubated overnight at 4 °C. Further, to block the wells, 250 μ L of 1 % (w/v) Bovine Serum Albumin (BSA) in PBS added and incubated at room temperature for 1 h. The 96 plate wells then washed thrice with PBS.

Initially, quinoline derivatives (25-250 μ g/mL) added to the collagen-coated wells and incubated for 15 min, prior to adding PRP, wells washed thrice with PBS. Then, the PRP pre-treated quinoline derivatives (25-250 μ g/mL) added to the collagen-coated wells. Each well of reaction mixture volume adjusted to 250 μ L by adding PBS and incubated at 37 °C. After 2 hours of incubation, the well washed thrice with PBS. Further, the adherent platelets were lysed

with 200 μL lysis buffer (100 mM citrate buffer (pH 5.4) having 0.1 % Triton X-100 and 5 mM *p*-nitrophenyl phosphate) at 37 °C for 90 min. The reaction arrested by adding 200 μL of 2N NaOH (stopping reagent) which is inactivating the platelet membrane acid phosphatase activity and the resultant color produced measured at 405 λ_{max} . Platelet adhesion was expressed in % adhesion, by considering the PBS-added platelet suspension as 100 percent.

HRBC based hemolysis assay (Hypotonicity induced hemolysis)

Thrombin playing an important role in acute and chronic inflammation [40-42]. Thrombin can amplify inflammation induced by other stimuli, either through ischemia. Thrombin, a key factor in coagulation and inflammation, typically elicits cellular responses via activation of protease-activated receptors (PARs). Thrombin has a well-characterized pro-inflammatory action that has recently been suggested to occur *via* activation of its receptor, the proteinase-activated receptor-1 (PAR1) [43,44]. The anti-inflammatory potential of quinoline derivatives evaluated by means of hypotonic induced (using distilled water) hemolysis assay [45-48]. The hypotonic solution (5 ml) having sorted the dosages of the quinoline derivatives (25-250 $\mu\text{g}/\text{ml}$) was used to assess the hemolysis in triplicates. 5 ml of distilled water (vehicle) and another 5 ml of indomethacin (250 $\mu\text{g}/\text{ml}$) used as the control respectively. 100 μL of Erythrocyte suspension was added to each tube, mixed thoroughly, and incubated for 60 min at 37 °C. Further, the mixture centrifuged for 5 min at 1200 g. The hemoglobin content of the supernatant measured at the absorbance (OD) range of 540 nm. The percentage hemolysis calculated by considering the hemolysis formed in distilled water as 100 %. The percent inhibition of hemolysis by the extract calculated thus:

$$\% \text{ Inhibition of hemolysis} = 1 - (\text{Ab}_2 - \text{Ab}_1 / \text{Ab}_3 - \text{Ab}_1) \times 100$$

Where,

Ab1 = absorbance of the test sample in isotonic solution

Ab2 = absorbance of the test sample in hypotonic solution

Ab3 = absorbance of control sample in hypotonic solution.

Cytotoxicity assessment of quinoline derivatives by MTT assay

The cell viability after reacting with the proposed quinoline derivatives was assessed by MTT [3-(4,5-dimethylthiazol-2-yl)-2,5-diphenyltetrazoliumbromide]. The current procedure adopted from our previous reports and modified accordingly [27-30]. In a 96 well microtiter plate, the Platelet-Rich Plasma (PRP) treated with 10 μ M Calcium Ionophore and quinoline derivatives (25-250 μ g/mL). PBS used to make the final volume of the reaction mixture up to 150 μ L and incubated at room temperature for 60 minutes, 150 μ M of MTT was added and incubated for another three hours. MTT separated and the obtained formazan crystals liquefied in DMSO and absorbance recorded at 570 λ_{max} using Tecan Sapphire multi-fluorescence microplate reader. The cell viability was calculated using the following formula,

$$\text{Cell viability (\%)} = \text{Mean OD/Control OD} \times 100 \%$$

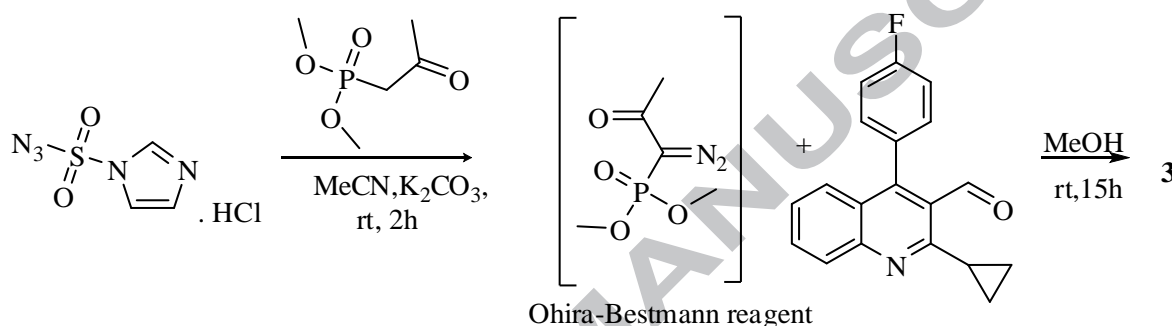
Statistical analysis

All results were expressed as a percentage increase or decrease with respect to control values. All results were compared by performing one-way ANOVA with Dunnett's post-test. GraphPad Prism version 7.1 for Windows, GraphPad Software, USA (www.graphpad.com) was used for statistical analysis.

Results and Discussion:

Synthesis of proposed 2-cyclopropyl-3-ethynyl-4-(4-fluorophenyl) quinoline (3):

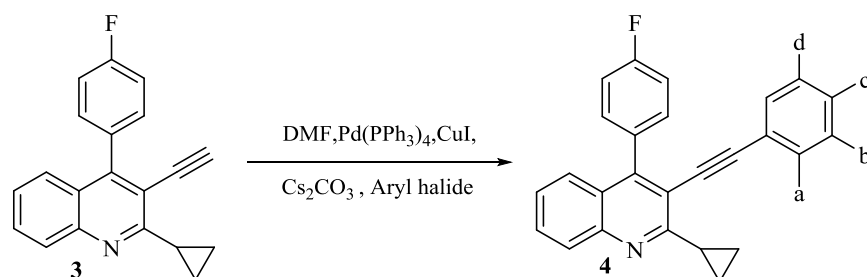
There are two synthetic routes were exploited to access desired compound **3**. In scheme-1, compound **3** prepared by Ohira-*Bestmann* reaction [49], in this one-pot synthesis, aromatic aldehyde was converted to alkyne. To achieve this, Ohira-*Bestmann* reagent was prepared from dimethyl-2-oxopropylphosphonate and imidazole-1-sulfonyl azide in the presence of K_2CO_3 in ACN followed by addition of the aldehyde (**1**) in methanol. After the reaction completed, the crude product was crystallized using isopropyl alcohol to get pure compound (**3**).



Scheme 1. Synthesis of proposed 2-cyclopropyl-3-ethynyl-4-(4-fluorophenyl) quinoline (**3**) using Ohira-Bestmann reaction

Synthesis of substituted 2-cyclopropyl-3-ethynyl-4-(4-fluorophenyl)quinoline derivatives (4a-l) from (3):

The derivatives of 2-cyclopropyl-3-ethynyl-4-(4-fluorophenyl)quinoline (**3**) was achieved as per the synthetic route displayed in Scheme 3 using Sonogashira coupling method. Table 1 depicts the substituents that were substituted on the scaffolds of 2-cyclopropyl-3-ethynyl-4-(4-fluorophenyl)quinoline (**3**). Compounds obtained in excellent yield up to 90 %. In addition, the molecular structure of the compound **3** was established by single-crystal X-ray diffraction studies. Then compound **3** subjected to Sonogashira Cross-Coupling Reaction (Scheme 2) with different aryl halides to get analogs of biologically active molecules [50-55]. The characterization data of newly synthesized compounds summarized in the experimental section. The computational studies carried out to confirm the medical efficacy of the molecule [56, 57].



Scheme 2. Synthesis of title compounds (4a-l) using Sonogashira Coupling

Table 1. Details of a to l of final products of scheme 3 (Sonogashira coupling)

S.No	Subtract (ArX)	Product	a	b	c	d
1	3-Bromo acetophenone	4a	H	CH ₃ CO	H	H
2	4-Bromo acetophenone	4b	H	H	CH ₃ CO	H
3	3-Bromo benzaldehyde	4c	H	CHO	H	H
4	4-Bromo chloro benzene	4d	H	H	Cl	H
5	Iodobenzene	4e	H	H	H	H
6	2-chloro-6,7-bis-(2-methoxyethoxy)quinoline	4f	-	-	-	-
7	2-Bromo 4-fluoro benzoic acid	4g	COOH	H	H	F
8	4-Bromo 3-methyl benzoic acid	4h	CH ₃	H	COOH	H
9	4-Bromo benzoic acid	4i	H	H	COOH	H
10	2-Bromo 5-iodo benzoic acid	4j	H	COOH	Br	H
11	5-Bromo 2-Chloro benzoic acid	4k	H	COOH	Cl	H
12	2-Bromo aceto phenone	4l	CH ₃ CO	H	H	H

The ORTEP representation with 50 % probability shown in **Fig. 3**, which clearly depicts a stable crystalline lattice structure of CEFQ. The single crystal X-ray studies (XRD) have shown that the crystal structure is triclinic with space group compound 3 (Table S1 & S2). The optimized molecular geometry of the isolated CEFQ molecule calculated using DFT at B3LYP/LAN 12dz level of theory and shown in **Fig.4a&b**. The calculated bond length and angles listed in Table S3 and compared with SXRD values. It found that most of the calculated values are higher than the experimental values because theoretical calculations carried for isolated gaseous state molecule whereas experimental ones are crystalline nature. Normally the C=N bond length in a heterocyclic ring is greater than 1.34 Å [58].

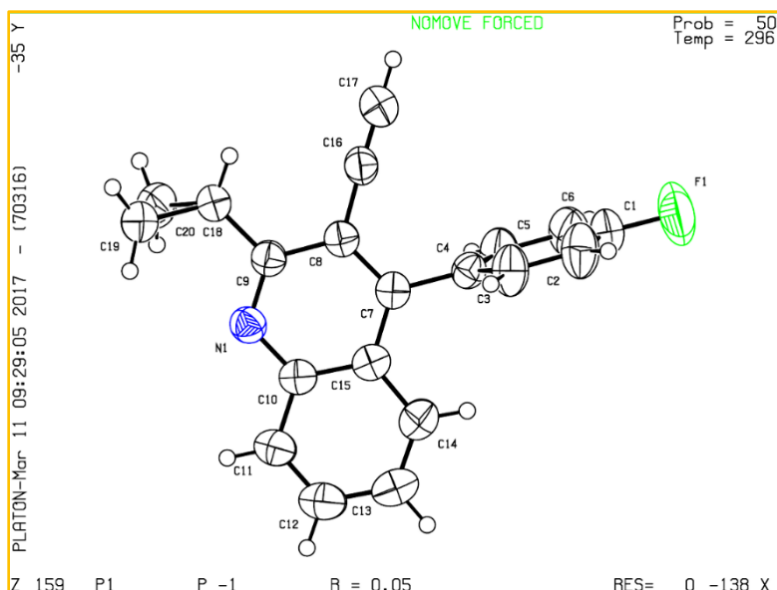


Figure 3. ORTEP structural analysis of 2-cyclopropyl-3-ethynyl-4-(4-fluorophenyl)quinoline (3).

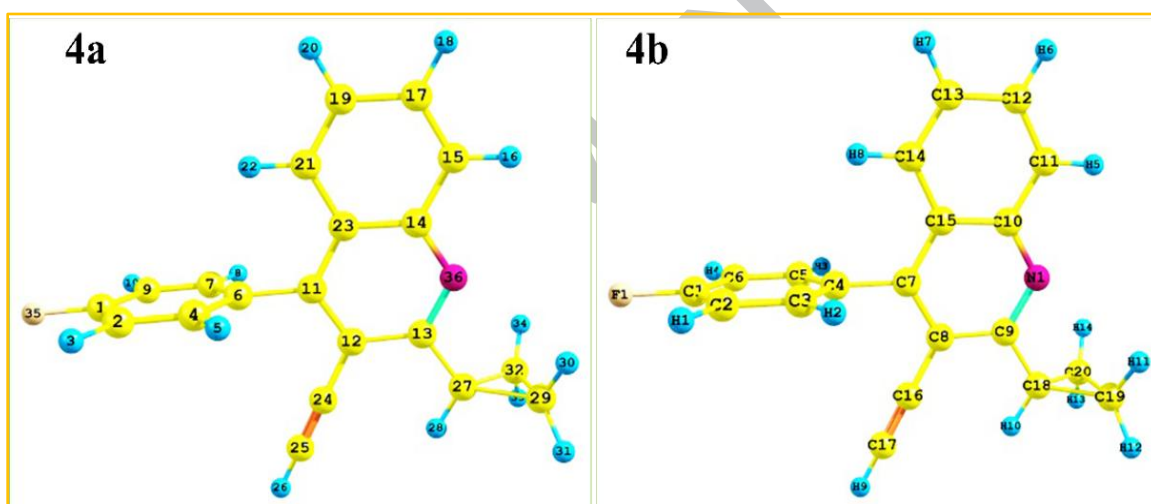


Figure 4a&b. optimized geometry of CEFQ for 2-cyclopropyl-3-ethynyl-4-(4-fluorophenyl)quinoline (3).

But in CEFQ the C=N (C9-N1) bond length is reduced to 1.336 Å due to the substitution of cyclopropyl ring at the second position. The C-C bond lengths are in the range of 1.397-1.412 Å and 1.389-1.439 Å in fluoro-substituted benzene ring and quinoline aromatic ring respectively. In the case of a heterocyclic ring, the length is 1.439 Å for C10-C15, C7-C15 bonds, 1.404 Å for C7-C8 and 1.454 Å for the C8-C9 bond. The weakening of C8-C9 bond length is mainly due to the substitution of cyclopropyl and ethyne group at respective carbon atoms. The ipso C-C-C

angles of such as C8-C7-C15 (118.9°), C7-C8-C9 (119.3°) and C8-C9-N1 (121.7°) of quinoline ring show deviation from the normal C-C-C (120°) value. Among these, the positive deviation (1.7°) of C8-C9-N1 is mainly due to the ring strain of cyclopropyl ring and the negative deviation (1.1°) of C8-C7-C15 attributed to a fluoro-substituted benzene ring.

3.2 Molecular electrostatic potential (MEP)

Molecular electrostatic potential is one of the useful ways to explore the electrostatic interaction in hydrogen bonding and to study the biological recognition process [59]. Electrostatic potential (ESP) correlates dipole moment, electronegativity, partial charges at the site of chemical reactivity of the molecule. In ESP diagram, the negative electrostatic potential (red color) corresponds to an attraction of the proton by the high electron density in the molecule and the positive electrostatic potential (blue color) corresponds to the repulsion of the proton by atomic nuclei in regions where low electron density exists and the nuclear charge is incompletely shielded. This electrostatic potential surface depicts the size, shape, charge density and electrophilic and nucleophilic reactivity site of the molecule. The increasing order of electron potential is blue < green < yellow < orange < red.

It inferred from the ESP diagram of CEFQ shown in **Fig. 5** that the maximum negative potential noted over heterocyclic nitrogen atom N1 and F1 that favors the electrophilic attack. The proton affinity of these atoms clearly visible from red region and mostly assisted by a lone pair of electrons. Therefore, these sites route the hydrogen bond interactions. The positive potential (blue color) shows the acceptor nature. The maximum positive region is located on the ethyne CH and aromatic CH, this confirms the nucleophilic attacking nature of these atoms.

From MEP, it inferred that N1, F1 atoms would bind with the electrophilic centers in proteins while the aromatic and ethyne CH groups favorably attacked by the nucleophile of the protein.

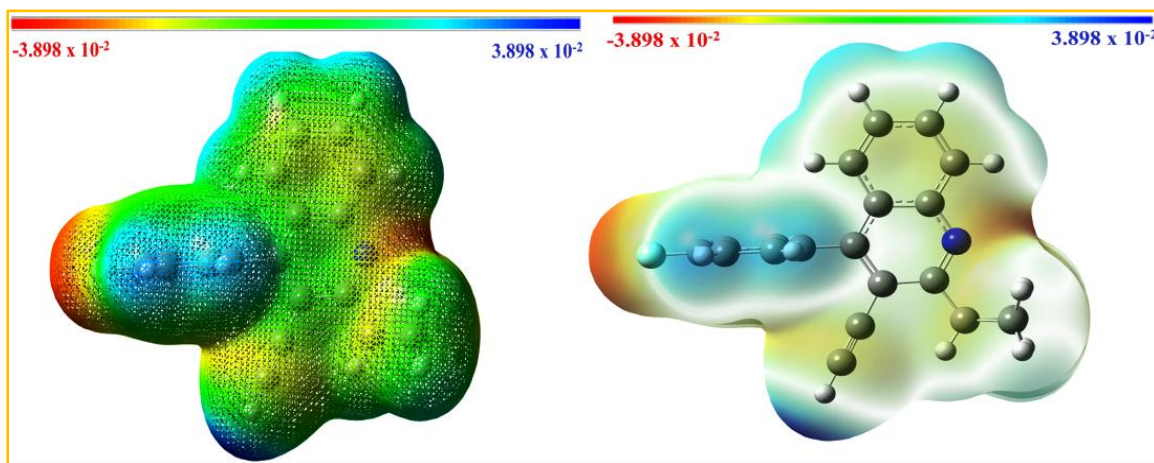


Figure 5. ESP diagram of CEFQ

3.3 Mulliken charge analysis

The Mulliken population analysis of atomic charge calculated by the density functional theory method. Fig. 6 shows the plot of the Mulliken atomic net charges in CEFQ. The negative charge accumulation over the F1 (-0.2429 e) and N1 (-0.0594 e) atoms show its electron donating nature. It clearly recognized by MEP shows negative potential over these atoms. All hydrogen atoms are a positive charge, out of which atom H9 (0.2844 e) possess the highest value. Usually, the hydrogen atom of the ethyne group is highly polarized one due to its attachment with high electronegative nature of terminal carbon. The large accumulation of negative charge on the carbon C17 (-0.4762 e) reveals its electronegative nature. Similarly, atom C1 (0.3172 e) possess the highest value amongst the positively charged carbon atoms owing to its association with the electronegative F1 atom. The cyclopropane ring carbons C19, C20 (-0.4514 e) also possess a high negative charge also reveals its electronegativity.

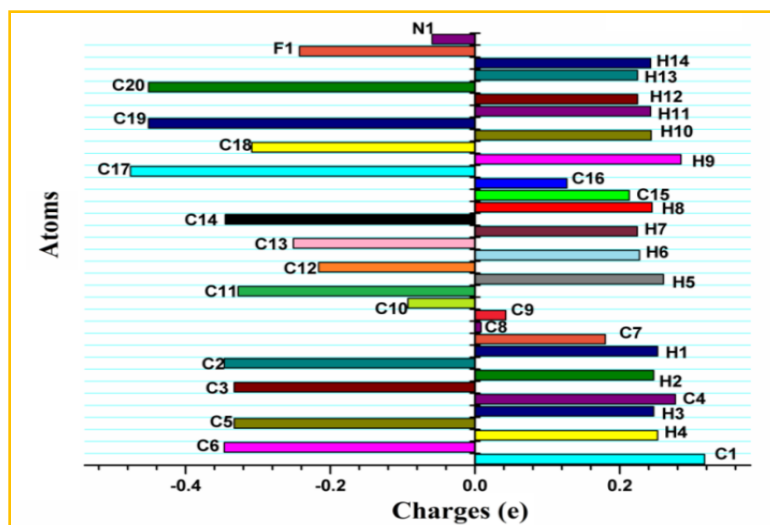


Figure 6. The plot of the Mulliken atomic net charges in CEFQ

3.4 Frontier molecular orbital analysis

In CEFQ, both HOMO and LUMO are delocalized over the quinoline ring, cyclopropyl and ethyne fragment but maximum electron density is spread over the aromatic C=C. HOMO-LUMO energy gap is found to be 4.467 eV (Fig. 7). The HOMO→LUMO transition implies an electron density transfer occur within quinoline ring and cyclopropyl fragment, especially within aromatic conjugation of CEFQ. DFT based descriptors help to understand the structure of molecules and their reactivity. Using HOMO and LUMO orbital energies, the ionization energy and electron affinity can be expressed as $I = -E_{\text{HOMO}}$, $A = -E_{\text{LUMO}}$ [60] and the global chemical reactivity descriptors of molecules such as hardness (η), chemical potential (μ) [61], softness (S), electronegativity (χ), electrophilicity index (ω) and additional electronic charge ΔN_{max} have been defined [62]. The hardness of the molecule is, $\eta = (I-A)/2$. The chemical potential of the molecule is, $\mu = -(I+A)/2$. The softness of the molecule is, $\zeta = 1/2\eta$; Electronegativity of the molecule is, $\chi = (I+A)/2$; The electrophilicity index of the molecule is, $\omega = \mu^2/2\eta$; Additional electronic charge, $\Delta N_{\text{max}} = -\mu/\eta$; Total energy change, $\Delta E_{\text{T}} = \eta/4$.

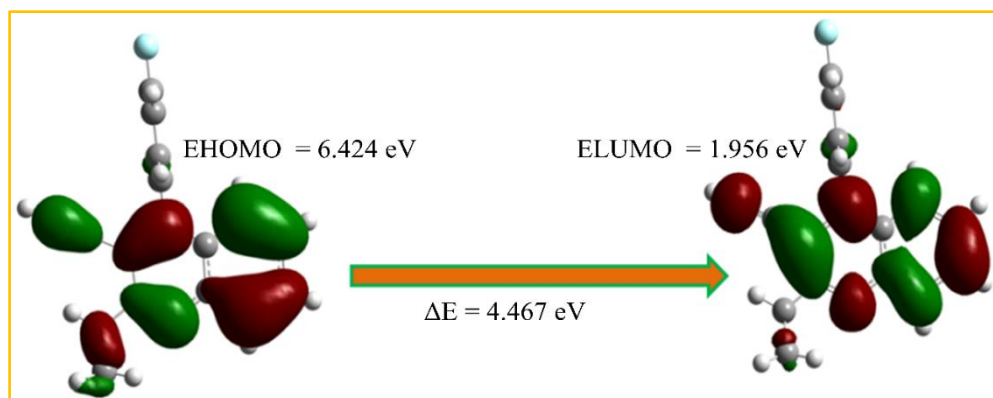


Figure 7. HOMO-LUMO energy gap of compound 3

Table 3. Frontier molecular orbital analysis of 2-cyclopropyl-3-ethynyl-4-(4-fluorophenyl)quinoline (**3**)

Descriptions	Values
E_{HOMO}	-6.424 eV
E_{LUMO}	-1.956 eV
Band gap energy, ΔE	4.467 eV
Ionization potential, I	6.424 eV
Electron affinity, A	1.956 eV
Hardness, η	2.234
Chemical potential, μ	-4.19
Softness, ζ	0.2238
Electrophilicity index, ω	3.929
Electronegativity, χ	4.19
Additional electronic charge, ΔN_{max}	1.875
Total energy change, ΔE_{T}	0.5585

Table 3 presents the energies of frontier molecular orbitals, ionization potential, electron affinity, hardness, chemical potential, softness, electrophilicity index, electronegativity and additional electronic charge of CEFQ. The smaller energy gap of CEFQ implies its low stability and it more polarizable which is associated with a high chemical reactivity. As it has low stability, CEFQ referred to as a soft molecule. The chemical hardness of the molecule related to the polarizability because a decrease of the energy gap makes easier polarization of the molecule [63]. The negative value of chemical potential indicates it is the ability of a system to resist the deformation of electron cloud under small perturbation during the chemical process. The hardness and softness of the molecule depending on the molecular orbital energies.

Electrophilicity index measures the stabilization energy when the system acquires an additional electronic charge from the surrounding and it resists the system to exchange electronic charge with the surrounding.

Molecular docking studies

Molecular docking study was executed in order to recognize the binding affinity and molecular interaction between present study quinoline derivatives (**4a-l**) to PAR1 (PDB ID: 3VW7) and PI3 Kinase (PDB ID: 3T8M). Least binding energy, binding affinity (k_i , the inhibitory constant) and ligand efficiency considered in narrowing the drug efficacy of **4a-l**. Table 4 depicts the obtained molecular mechanistic values from molecular docking studies. Initially, to scrutinize the most efficacies compounds and most selectively scored receptors; we have summated and averaged the molecular mechanistic values. With an average least binding energy (-10.03 kcal/mol), ligand efficiency (-0.35) and binding affinity (0.56 μ M), compounds **4a-l** showed a most fortunate activity selectiveness over PI3 Kinase (PDB ID: 3T8M). Meanwhile, we have also observed noteworthy molecular mechanistic values against PAR1 (PDB ID: 3VW7).

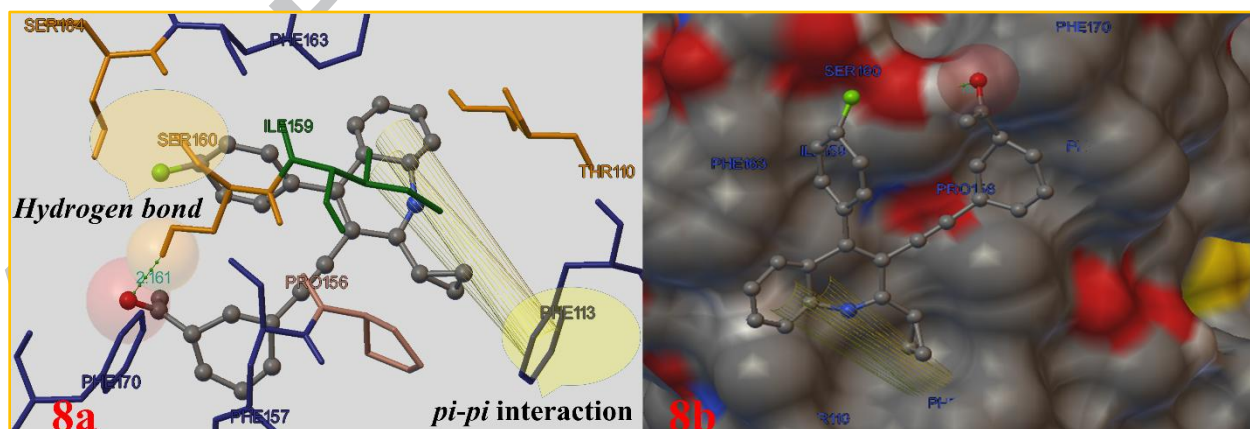


Figure 8a. Molecular interaction of **4a** to PI3 Kinase (PDB ID: 3T8M) **Figure 8b.** Compound **4a** into the binding pocket (active site) of PI3 Kinase (PDB ID: 3T8M)

Except for **4d** and **4h**, remaining all compounds were showed good binding affinity with an inhibitory constant (*ki*) range of 0.056 to 0.813 μM . Based on this molecular docking study results, we have screened the compounds **4a-c**, **4e-g**, and **4i-l** for further PI3 kinase enzyme inhibition studies. In addition, we have validated the molecular interactions of best-docked compounds to corresponding receptors PI3 Kinase (PDB ID: 3T8M). Fig. 8a&b is depicted as the pictorial representation of the molecular interaction between PI3 Kinase (PDB ID: 3T8M) and most potent PI3 Kinase inhibitor (**4a**) among **4a-l**. The established non-covalent (π - π interaction between aryl ring of **4a** to the Phe113 amino acid residue of PI3 Kinase) and hydrogen bond (between the oxygen moiety of acetoxy group of compound **4a** and PI3 kinase) was the source of evidence to the drug action of **4a** (Fig. 8a). The inhibition, perhaps, facilitated by these non-covalent and hydrogen bonding. In the acetoxy group, the acetyl end is a weekly deactivating group, thus, the possibility of further biological reaction also less. One of the $-\text{OH}^{[+]}$ group of Serine being the donor and the acceptor is acetoxy group's $-\text{O}^{[-]}$ of **4a** (Fig. 8b).

Table 4. Molecular mechanistic values of molecular docking results

Entry	Binding energy (kcal/mol)		Ligand efficiency		Inhibitory constant (<i>ki</i>) μM)	
	3VW7	3T8M	3VW7	3T8M	3VW7	3T8M
4a	-6.99	-11.73	-0.23	-0.44	7.52	0.056
4b	-8.27	-11.12	-0.27	-0.41	0.868	0.086
4c	-7.94	-10.86	-0.25	-0.40	3.56	0.094
4d	-5.96	-7.21	-0.21	-0.25	42.46	1.242
4e	-6.35	-9.06	-0.23	-0.28	22.25	0.468
4f	-7.11	-10.20	-0.17	-0.37	6.11	0.174
4g	-8.01	-11.33	-0.26	-0.44	1.4	0.075
4h	-4.16	-7.60	-0.25	-0.23	68.45	2.512
4i	-7.66	-9.98	-0.27	-0.31	2.44	0.357
4j	-9.28	-11.63	-0.27	-0.43	0.392	0.060
4k	-7.91	-9.82	-0.21	-0.30	1.024	0.842
4l	-7.71	-9.87	-0.29	-0.32	2.62	0.813
Sum	-87.35	-120.41	-2.91	-4.18	159.094	6.779
Average	-7.27917	-10.0342	-0.2425	-0.34833	13.25783	0.564917

Results of PI3 Kinase inhibition studies

In recent days, to prevent arterial ischemic incidence, targeting GPCRs mediated intracellular signaling downstream with PI3kinase being the novel tactics [64]. In fact, even though the mechanism is unclear, thrombin proteolytic effect of PAR-1 activates PI3K and Akt, known to play an essential role in proliferation (Fig. 9) [65]. Thus, the inhibition of PI3Kinase is essential to prevent the downregulation of cellular activity through GPCRs and PAR-1 activities. In this study, as indicated by molecular docking results, PI3Kinase inhibition activity evaluated for the compounds **4a-c**, **4e-g**, and **4i-l**. The assay repeated thrice in triplicates and the compounds diluted at various concentration (25-250 $\mu\text{g/mL}$). The results were expressed in relative % activity and the IC_{50} values in μM . We used Wortmannin as the standard drug to assess the inhibitor/drug efficacy of these compounds. In a recent study, Wortmannin showed 55.4 % thrombin-induced basal phosphorylation reduction of Thr308 with 70.1 % thrombin inhibition [65].

In addition to this, Akt (a serine-threonine kinase) was found as part of a Wortmannin-sensitive signaling pathway in the downstream activity of PI3kinase [66,67]. To unveil the PI3 kinase inhibition efficacy of compounds **4a-c**, **4e-g**, and **4i-l**, we have analyzed the inhibition assay results in a various point of views. Fig. 10a-d illustrating the results of relative % activity, dose-responsive activity, 50 % amount of compound needed to have maximum inhibition activity (IC_{50}) and the comparison of *in silico* and *in vitro* activity result's resemblances. The relative percentage activity was measured by testing the inhibitory potentials of compounds and the standard drug at various concentrations (n=4). As depicted in Fig. 10a compounds **4a**, **4b**, and **4j** showed slightly increased activity while remaining compounds showed lesser activity than the standard, Wortmannin. With a maximum of 72.57 ± 5.84 % (mean value) of % inhibition

was the best achieved by 4a than Wortmannin (mean value of 67.25 ± 3.84 %). Compounds **4b** and **4j** were also showed higher values as 68.98 ± 4.87 % and 68.52 ± 3.94 % respectively than the standard. We found a dose depended on increased activity up to a concentration of 10^{-6} (Fig. 10b).

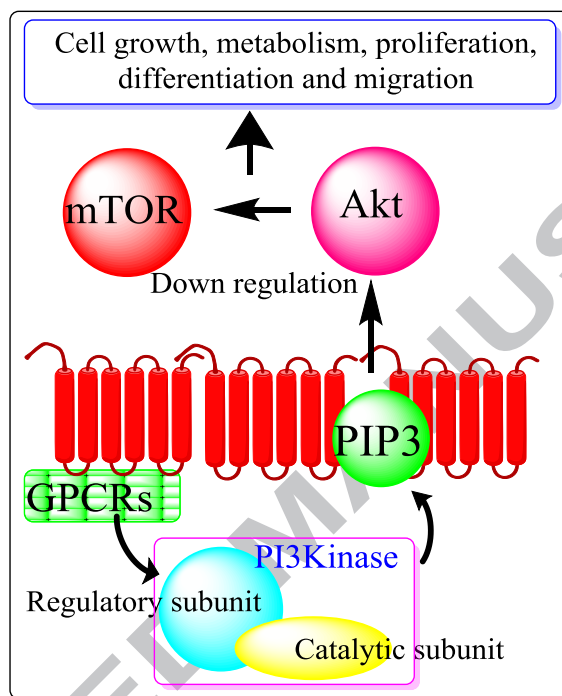


Figure 9. The role of GPCRs in the activation of PI3Kinases, known to play an essential role in proliferation. **Note:** GPCRs involving in the activation of PI3K to the plasma membrane and it catalyzes the formation of PIP3 from phosphatidylinositol-4,5-bisphosphate (PI-4,5-P₂). PIP3 acts on a range of downstream effectors to promote cellular responses including proliferation and migration by involving in the Akt/mTOR activation.

In that concentration, **4a** was able to inhibit the PI3Kinase up to 90.85 ± 2.86 % while the standard showed little lower value (86.12 ± 3.48 %). The calculated IC₅₀ values (mean) displayed in Fig. 10c. **4a** was able to inhibit PI3Kinase with the lowest molar quantity (IC₅₀ = 0.45 ± 0.025 μM). Wortmannin has reached its maximum activity at an IC₅₀ of 0.75 ± 0.05 μM while compounds **4b** and **4j** were required almost the same amount of IC₅₀ of the standard. We displaying Fig. 10d to compare the *in silico* and *in vitro* results and to validate the reliability of the proposed PI3Kinase activity. As showed in Fig. 10d, compounds **4a**, **4b**, **4g**, and **4j** were best

compounds to score significant molecular mechanistic values also found best for the PI3Kinase activity. Thus, the reliability between the *in silico* and *in vitro* activity found virtuous.

In vitro thrombolytic activity results of compounds 4a, 4b, 4g, and 4j

Thrombin is one of the main factors in the development of various diseases. Thrombin induces PAR-1 gene expression in endothelial cells via activation of Gi-linked Ras/Mitogen-activated protein kinase pathway [68]. In the present study, the clot lysis activity of compounds 4a, 4b, 4g, and 4j assessed to quantify their thrombolytic effects. After treating the compounds and standard drug, the dry weight of the vial considered as the result by discarding the serum released due to the thrombin degradation in every 15 minutes.

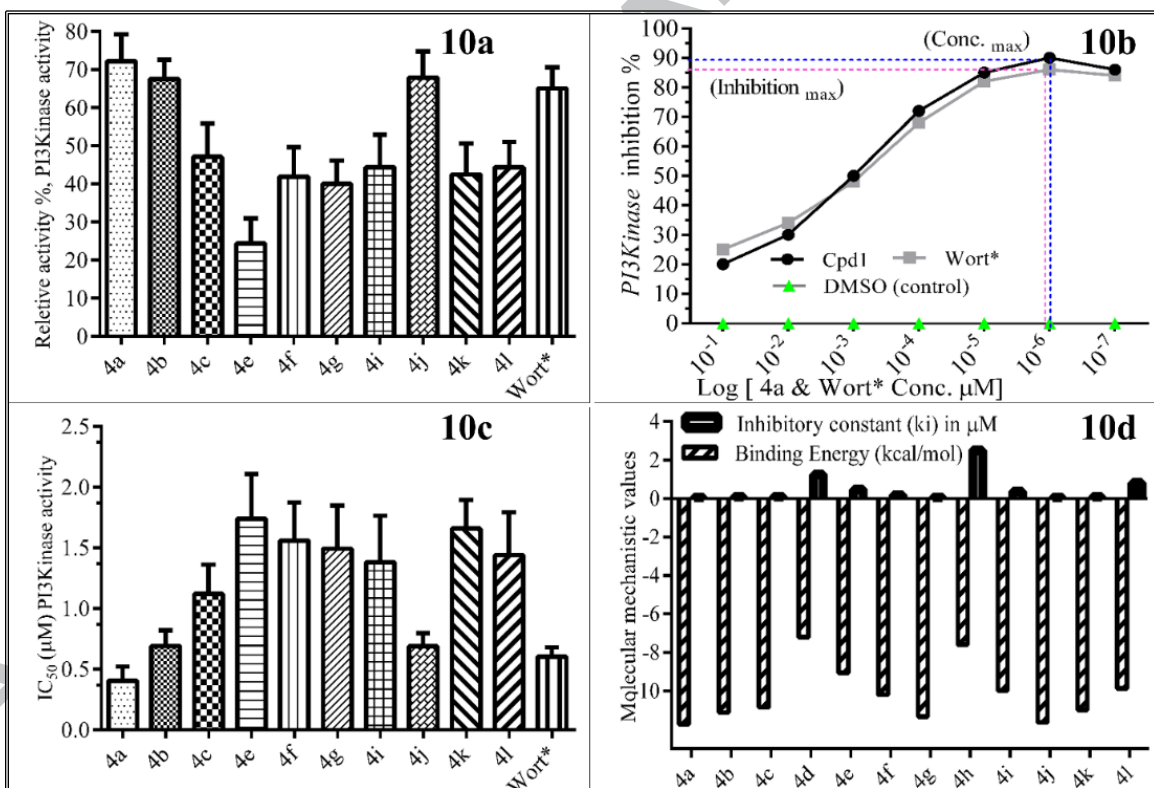


Figure 10a-d. Results of PI3Kinase inhibition assay. **Figure 10a.** Relative percentage activity results of compounds 4a-c, 4e-g, 4i-l and Wortmannin. **Figure 10b.** Dose-response curve of compounds 4a and Wortmannin. **Figure 10c.** Calculated IC₅₀ (μM) values of compounds 4a-c, 4e-g, 4i-l, and Wortmannin. **Figure 10d.** Molecular mechanistic values of docking results in order to compare *in vitro* and *in silico* results reliability.

As anticipated compounds, **4a** (95 % lysed) and **4j** (90 % lysed) found as most effective thrombolytic agents. They lysed the whole blood clot within the third quarter of the first hour while streptokinase (standard) (86 % lysed) taken more than 90 min to complete the process. Also, it was noticed that there was no change or ups and downs in the lysis activity on the blood samples which were collected from three set of age group (15-25 (n=6); 26-36 (n=6); 37-50 (n=6)) and 51 above (n=6).

Effect of compound **4a** on agonist-induced platelet aggregation and platelet adhesion

Platelets are the key mediators in maintaining the integrity of the endothelium. Guanine nucleotide-binding proteins (G proteins) are able to interact precisely with numerous functionally different heterotrimeric. Thus, agonist-activated GPCRs can persuade various signaling pathways to alter normal cellular activities [69,70]. We have tested the effect of compound **4a** on platelet aggregation and platelet adhesion with agonist-induced platelets. In order to stimulate platelet aggregation collagen/ADP/epinephrine used as an agonist.

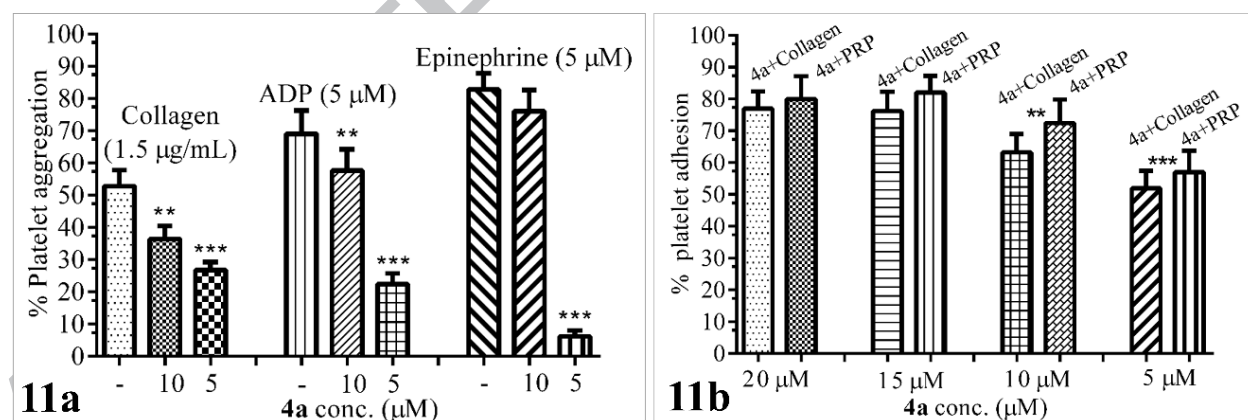


Figure 11. Effect of compound **4a** on (a) Platelet aggregation induced by Collagen/ADP/Epinephrine and (b) Platelet adhesion on immobilized collagen type I with compound **4a** pre-treated collagen and PRP pre-treated with compound **4a**. Values are presented as mean \pm SEM (n=5), expressed as the percentage decrease in aggregation and increase in platelet adhesion. ** p <0.01, *** p <0.001; significant compared to control.

In the results, in general, **4a** showed its maximum platelet aggregation and adhesion activity in low concentration itself, while increasing the concentration, there was no improvement in the

activity. Compound **4a** showed a significant agonist-induced platelet aggregation inhibition. The epinephrine-induced aggregation suppressed by compound **4a** at 5- μ M concentration. In contrast, there was no remarkable platelet aggregation activity while testing the compound **4a** alone (Fig. [11a](#) & Fig. [11b](#)).

Effect of compound **4a** on Hypotonicity induced hemolysis of HRBCs

Data from Table show that compound **4a** significantly ($p \leq 0.05$) inhibited lysis induced by water. This showed by the high percentage inhibition of hemolysis (95.52 %, 85.56 %, and 68.34%) obtained for doses of 2.5, 5 and 10 μ M respectively. The inhibition of hemolysis was found to be dose dependent, decreased with increased concentration started from 10 μ M at the beginning of compound **4a** in DMSO and was comparable with indomethacin, the standard (Table 5).

Table 5. Effect of compound **4a** extract on Hypotonicity induced hemolysis of HRBCs

Treatment	Conc. (μ g/mL)	Mean absorbance \pm SD		% inhibition of hemolysis
		Hypotonic solution	Isotonic solution	
Control	-	0.65 \pm 0.21	0.03 \pm 0.01	-
4a	250	0.54 \pm 0.18	0.04 \pm 0.03	18.8 \pm 1.87
	200	0.40 \pm 0.11	0.07 \pm 0.33	20.3 \pm 2.86
	150	0.24 \pm 0.06*	0.18 \pm 0.06	50.8 \pm 4.28
	100	0.21 \pm 0.05*	0.05 \pm 0.04	73.3 \pm 3.83
	50	0.19 \pm 0.04*	0.02 \pm 0.01	88.8 \pm 2.47
Indomethacin	200	0.28 \pm 0.02*	0.03 \pm 0.01	76.7 \pm 3.48

Level of Significance * = $p < 0.05$. Percent inhibition of hemolysis calculated relative to control.

Results of Cytoprotective effects of compound **4a**

In order to investigate whether **4a** had a cytoprotective effect, MTT assay performed. Calcium Ionophore (A23187) used as a standard agonist, which reduced cell viability from 93 % to 21 %. However, treating platelets with **4a** restored its survivability up to 75 % in agonist-activated platelets.

Conclusion

In the present study, few novel quinoline derivatives synthesized and evaluated as GPCR ligands via PI3Kinase inhibition, a thrombolytic assessment that supported through platelet aggregation and adhesion activities. We focused on the established molecular mechanistic values to **4a-l** with optimal combinations of physicochemical properties and pharmacological properties. Among all compounds, perhaps, the main drawback for the impotency of **4f** (3-((6,7-bis(2-methoxyethoxy)quinoline-2-yl)ethynyl)-2-cyclopropyl-4-(4-fluorophenyl)quinoline, (C₃₅H₃₁FN₂O₄)) due to relatively high molecular weight (562.6414) while comparing to other compounds among **4a-l**. Also their predicted Boiling Point: 1365.35 [K], Melting Point: 1072.64 [K], Log P: 6.93, CLogP: 7.56239, LogS -8.206 found to exceed from the limit). Remaining all compounds were effective for the proposed activities in this study. **4a**, **4b**, **4g**, and **4j** are compounds that potentially identified and recommended for further drug evaluation against the proposed studies here.

Acknowledgment

The authors are deeply acknowledging Research & Development Centre, Bharathiar University, Coimbatore - 641046, India.

References:

1. Kumar S, Bawa S, Gupta H. Biological activities of quinoline derivatives. *Mini Rev Med Chem.* 9 (2009) 1648-54.
2. Shweta J, Vikash C, Pankaj K.Jain, Kamla P, Devendra P, Ankur V, Comprehensive review on current developments of quinoline-based anticancer agents, *Arabian Journal of Chemistry*, (2016) <https://doi.org/10.1016/j.arabjc.2016.10.009>.

3. Gopaul K, Shintre SA, Koorbanally NA1. A Review on the Synthesis and Anti-cancer Activity of 2-substituted Quinolines. *Anticancer Agents Med Chem.* 15 (2015):631-46.
4. Kitagawa W, Tamura T. A quinoline antibiotic from *Rhodococcus erythropolis* JCM 6824. *J Antibiot (Tokyo).* 61 (2008) 680-2.
5. Nafees A, Keyur G.B, Sudeep S, Debashis M, Inder Pal S, Kamlesh K.B. Synthesis and anti-HIV activity of alkylated quinoline 2,4-diols. *Bioorg Med Chem.* 18 (2010) 2872-2879.
6. W. David H, Peter D.G, Suet C.L, Richard A, Paul A.S, Andrew S, Pedro H, Maria L. S.C, Alison E.S, Darren M, Alison A, Raman S, Ashley J.W, Paul T. P.B, Nicholas E.F, Ghaith A, Sally M, Maxine C, Neil G.B, Stephen A.W, Giancarlo A.B, Paul M. O'Neill, and Gemma L.N. Rational Design, Synthesis, and Biological Evaluation of Heterocyclic Quinolones Targeting the Respiratory Chain of *Mycobacterium tuberculosis*. *J. Med. Chem.* 60 (2017) 3703–3726.
7. Peter N and Scott K. Treatment of acute vivax malaria with tafenoquine. *Trans R Soc Trop Med Hyg.* 99 (2005) 2-5.
8. Mukherjee S, Pal M. Medicinal chemistry of quinolines as emerging anti-inflammatory agents: an overview. *Curr Med Chem.* 20 (2013) 4386-410.
9. Muruganantham N, Sivakumar R, Anbalagan N, Gunasekaran V, Leonard JT. Synthesis, anticonvulsant and antihypertensive activities of 8-substituted quinoline derivatives. *Biol Pharm Bull.* 27 (2004) 1683-7.
10. Sumesh E, Airody VA, Imran HC, Nishith KP, KD Thomas. New quinoline derivatives: Synthesis and investigation of antibacterial and antituberculosis properties. *Eur. J. Med. Chem.* 45 (2010) 3374-3383.

11. Timothy M. E.D, Lawrence G.D, Sally A.K, Benjamin J.H, Robert G.H, Kevin T.B. Neurological, cardiovascular and metabolic effects of mefloquine in healthy volunteers: a double-blind, placebo-controlled trial; *British Journal of Clinical Pharmacology*, 42, (1996) 415–421.
12. Seyferth D, Marmor R.S, Hilbert P. Reactions of dimethylphosphono-substituted diazoalkanes. (MeO)₂P(O)CR transfer to olefins and 1,3-dipolar additions of (MeO)₂P(O)C(N₂)R. *J. Org. Chem.* 36 (1971) 1379-1386.
13. Gilbert, J. C.; Weerasoriya, U. Diazoethenes: their attempted synthesis from aldehydes and aromatic ketones by way of the Horner-Emmons modification of the Wittig reaction. A facile synthesis of alkynes. *J. Org. Chem.* 47 (1982) 1837-1845.
14. A. Elangovan, Y.-H. Wang, T.-I. Ho, Sonogashira Coupling Reaction with Diminished Homocoupling. *Org. Lett.*, 5 (2003) 1841-1844.
15. M. Eckhardt, G. C. Fu, The First Applications of Carbene Ligands in Cross-Couplings of Alkyl Electrophiles: Sonogashira Reactions of Unactivated Alkyl Bromides and Iodides *J. Am. Chem. Soc.*, 125 (2003) 13642-13643.
16. McCoy KL, Gyoneva S, Vellano CP, Smrcka AV, Traynelis SF, Hepler JR. Protease-Activated Receptor 1 (PAR1) coupling to G_{q/11} but not to G_{i/o} or G_{12/13} is mediated by discrete amino acids within the receptor second intracellular loop. *Cellular Signalling*. 24 (2012) 1351-1360.
17. McEachron TA, Pawlinski R, Richards KL, Church FC, Mackman N. Protease-activated receptors mediate crosstalk between coagulation and fibrinolysis. *Blood*. 116 (2010) 5037-44.

18. Magnus N, Garnier D, Rak J. Oncogenic epidermal growth factor receptor upregulates multiple elements of the tissue factor signaling pathway in human glioma cells. *Blood*. 116 (2010) 815-818.
19. Rong Y, Belozarov VE, Tucker-Burden C, et al. Epidermal growth factor receptor and PTEN modulate tissue factor expression in glioblastoma through JunD/activator protein-1 transcriptional activity. *Cancer Res*. 69 (2009) 2540-2549.
20. Macrae C.F, Bruno I.J, Chisholm J.A, Edgington P.R, McCabe P, Pidcock E, Rodriguez-Monge L, Taylor R, Wood P.A, Van de S.P.A., Mercury CSD 2.0—New Features for the Visualization and Investigation of Crystal Structures. *J. Appl. Crystallogr*. 41 (2008) 466-470.
21. M. J. Frisch, G. W. Trucks, H. B. Schlegel, G. E. Scuseria, M. A. Robb, J. R. Cheeseman, G. Scalmani, V. Barone, B. Mennucci, G. A. Petersson, et al. Gaussian 09, Revision E.01, Inc., Wallingford CT, (2009).
22. G.A. Zhurko, CHEMCRAFT, Version: 1.7 (build 365) (<https://www.errorfix-pc.com/filedatabase/english/Chemcraft.exe/1.7.0.365>)
23. Coughlin SR. Thrombin signaling and protease-activated receptors. *Nature* 407 (2000) 258–264.
24. Ossovskaya VS, Bunnett NW, de Garavilla L, Vergnolle N, Young SH, Ennes H, Steinhoff M, D'Andrea MR, Mayer EA, Wallace JL, Hollenberg MD, Andrade-Gordon P. Protease-activated receptors: contribution to physiology and disease. *Physiol Rev* 84 (2004) 579–621.
25. Koyasu, S. The role of PI3K in immune cells. *Nat. Immunol*. 4 (2003) 313–319.

26. Harissios V. Thrombin Induces Mast Cell Adhesion to Fibronectin: Evidence for Involvement of Protease-Activated Receptor-11. *The Journal of Immunology*, 169 (2002) 4551–4558.
27. Rajesh KM, Manikandan A, Violet DV. N-substituted Hydroxynaphthalene imino-oxindole derivatives as a new class of pi3-kinase inhibitor and breast cancer drug: Molecular validation and Structure-Activity Relationship studies. *Chem Biol Drug Des.* 91 (2018) 277–284.
28. Manikandan A, Sivakumar A. Molecular explorations of substituted 2-(4-phenylquinolin-2-yl) phenols as phosphoinositide 3-kinase inhibitors and anticancer agents. *Cancer Chemother Pharmacol* 79 (2017) 389-397.
29. Vivek P.M, Manikandan A, Sivakumar A and Sathiyarayanan K.I. Molecular substantiation and drug efficacy of relatively high molecular weight S-BINOLs; appraised as breast cancer therapeutics and PI3Kinase inhibitors. *J. Heterocyclic Chem.*, 55 (2018) 1339–1345 DOI: 10.1002/jhet.3166.
30. Vivek P.M, Manikandan A, and Sathiyarayanan K.I. Iodine catalyzed three component synthesis of 1-((2-hydroxynaphthalen-1-yl)(phenyl)(methyl) pyrrolidin-2-one derivatives: rationale as potent PI3K inhibitors and anticancer agents. *Bioorg. Med. Chem. Lett.* 27 (2017,) 2510–2514.
31. Manikandan A, S Ravichandran, Kumaravel K, Sivakumar A, Rethna Priya. Molecular docking and in vitro evaluations of *Hippocampus trimaculatus* (seahorse) extracts as anti-inflammatory compounds. *Int. J. Bioinformatics Research and Applications*, 12 (2016) 355-371.

32. Manikandan A, Pearl M, Sathiskumar M, C Muñoz-Garay and Sivakumar A. Therapeutic investigations of novel Indoxyl-based indolines: A drug target validation and Structure-Activity Relationship of angiotensin-converting enzyme inhibitors with cardiovascular regulation and thrombolytic potential. *Eur. J. Med. Chem.* 141 (2017) 417-426.
33. Troy A. Mc. E, Rafal P, Kristy L.R, Frank C.C, Nigel M. Protease-activated receptors mediate crosstalk between coagulation and fibrinolysis. *Blood.* 116 (2010) 5037-5044.
34. Henri H.V, Florence S, Marjolein K, Lesley G.E, Andrade-Gordon P, Barbara M.M, Wolfram R. Protease-activated receptor (PAR) 2, but not PAR1, signaling promotes the development of mammary adenocarcinoma in polyoma middle T mice. *Cancer Res.* 68 (2008) 7219-7227.
35. Yang E, Boire A, Agarwal A, Nguyen N, O'Callaghan K, Tu P, Kuliopulos A, Covic L. Blockade of PAR1 signaling with cell-penetrating pepducins inhibits Akt survival pathways in breast cancer cells and suppresses tumor survival and metastasis. *Cancer Res.* 69 (2009) 6223-6231.
36. Silva, L.Lorenzo da; D'Amico, Elbio Antonio. Comparative study of platelet aggregation by turbidimetric and impedance methods in patients under acetylsalicylic acid antiplatelet therapy. *Rev. Bras. Hematol. Hemoter.* 32 (2010) 463-468.
37. Kumar MS, Girish KS, Vishwanath BS, Kemparaju K. The metalloprotease, NN-PF3 from *Naja naja* venom inhibits platelet aggregation primarily by affecting $\alpha 2\beta 1$ integrin. *Ann Hematol* 90 (2011) 569–577.
38. Nowak G, Wiesenburg A, Schumann A, Bucha E. Platelet adhesion assay--a new quantitative whole blood test to measure platelet function. *Semin Thromb Hemost.* 31 (2005) 470-5.

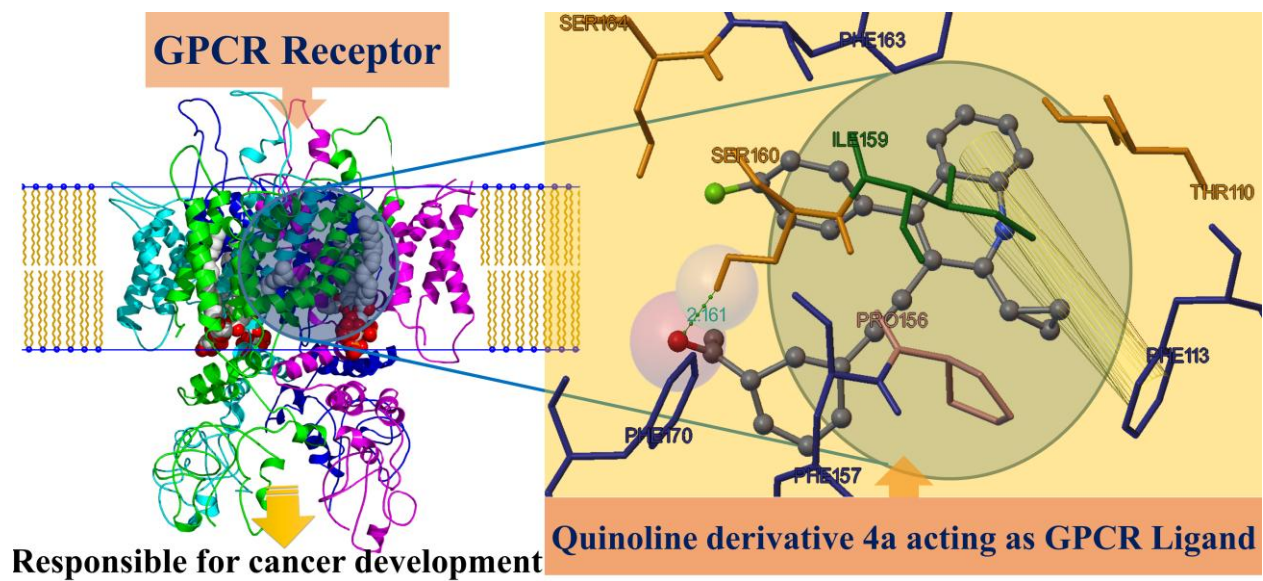
39. Bellavite P, Andrioli G, Guzzo P, Arigliano P, Chirumbolo S, Manzato F, Santonastaso C. A colorimetric method for the measurement of platelet adhesion in microtiter plates. *Anal Biochem* 216 (1994) 444–450.
40. Chen D, Dorling A. Critical roles for thrombin in acute and chronic inflammation. *J Thromb Haemost.* 7 (2009) 122-6.
41. Popović M, Smiljanić K, Dobutović B, Syrovets T, Simmet T, Isenović ER. Thrombin and vascular inflammation. *Mol Cell Biochem.* 359 (2012) 301-13.
42. Morris R, Winyard PG, Blake DR, Morris CJ. Thrombin in inflammation and healing: relevance to rheumatoid arthritis. *Annals of the Rheumatic Diseases.* 53 (1994) 72-79.
43. Vergnolle N, Morley DH, John LW. Pro- and Anti-Inflammatory Actions of Thrombin: A Distinct Role for Proteinase-Activated Receptor-1 (PAR1). *British Journal of Pharmacology* 126 (1999) 1262–1268.
44. Landis C. Why thrombin PAR1 receptors are important to the cardiac surgical patient. *J Extra Corpor Technol.* 39 (2007) 305-7.
45. Manikandan A, Ravichandran S, Sathiyarayanan K.I, Sivakumar A. Efficacy and rationale of 2-(4-phenylquinolin-2-yl)phenols as COX-2 inhibitors; an approach to emergent the small molecules as the anti-inflammatory and analgesic therapeutics. *Inflammopharmacology*, 25 (2017) 621–631.
46. Rajesh KM, Manikandan A, Violet DV. Synthesis and molecular drug efficacy of indoline based dihydroxy-thiocarbamides; inflammation regulatory property unveiled over COX-2 inhibition, molecular docking, and cytotoxicity prospects. *Journal of Heterocyclic Chemistry.* (2018) DOI: 10.1002/jhet.3201.

47. Manikandan A, Nemani SC, Sadheeshkumar V and Arumugam S. Spectroscopic investigations for photostability of Diclofenac sodium complexed with hydroxypropyl- β -cyclodextrin. *J App Pharm Sci*, 6 (2016) 098-103.
48. Thangarasu P, Manikandan A, Thamaraiselvi S. Discovery, synthesis and therapeutic efficacy of novel 3-O-methoxy-4-halo-disubstituted 5,7-dimethoxy chromans; small molecules with the ability of DNA gyrase inhibition, bacterial cell wall damage and antibacterial prospective. *Bioorg Med Chem*, 26 (2018) 3438-3452.
49. Tue HJ and Jesper LK. In Situ Generation of the Ohira–Bestmann Reagent from Stable Sulfonyl Azide: Scalable Synthesis of Alkynes from Aldehydes. *J. Org. Chem.*, 79 (2014) 9423-9426.
50. E. Vedejs, C. F. Marth. Mechanism of the Wittig reaction: the role of substituents at phosphorus. *J. Am. Chem. Soc.*, 110 (1988), 3948–3958.
51. Mira B, Bhartesh D, Ryan M, Avinash N.T. Terminal alkynes from aldehydes via dehydrohalogenation of (Z)-1-iodo-1-alkenes with TBAF. *Tetrahedron Letters* 49 (2008) 6794- 6796.
52. Masaru O and Yuji M. Conversion of Bromoalkenes into Alkynes by Wet Tetra-n-butyl ammonium Fluoride. *J. Org. Chem.*, 74 (2009) 442–444.
53. Zhe W, Silvio C, Guoyou X, Michael E.P, Joseph M.F, and Pat. N.C. A Practical Preparation of Terminal Alkynes from Aldehydes. *J.Org. Chem*, 65 (2000) 1889-1891.
54. Yoshihiro M, Yukiko H, Kayo S, Yoshifumi K, and Hiroshi I. Synthesis of 2-Alkenyl- and 2-Alkynyl-benzo[b]phospholes by Using Palladium-Catalyzed Cross-Coupling Reactions. *Org. Lett.*, 15 (2013), 4458–4461.

55. Rafael C and Carmen N. The Sonogashira Reaction: A Booming Methodology in Synthetic Organic Chemistry. *Chem. Rev.*, 107 (2007), 874–922.
56. Dapeng W, Dong Y, Daquan Z, Kang L, Lixin G, Tong L. Electrochemical and DFT studies of quinoline derivatives on corrosion inhibition of AA5052 aluminum alloy in NaCl solution, *Applied Surface Science*, 357, Part B (2015) 2176-2183.
57. Sonawane AD, Garud DR, Udagawa T, Koketsu M. Synthesis of thieno[2,3-b]quinoline and selenopheno[2,3-b]quinoline derivatives via iodocyclization reaction and a DFT mechanistic study. *Org Biomol Chem.* 16 (2018) 245-255.
58. N. Prabavathi, A. Nilufer, V. Krishnakumar, Quantum mechanical study of the structure and spectroscopic (FT-IR, FT-Raman, ^{13}C , ^1H , and UV), NBO and HOMO-LUMO analysis of 2-quinoxaline carboxylic acid. *Spectrochim. Acta A* 92 (2012) 325–335.
59. Bhaskaran S, Yohannan SM, Chacko YP, Somasekharan S, Stevan Ar, Sanja J.A, Christian VA, Badiadka N. Quinoline derivatives as possible lead compounds for anti-malarial drugs: Spectroscopic, DFT and MD study, *Arabian Journal of Chemistry* (2017) <https://doi.org/10.1016/j.arabjc.2017.07.006>.
60. Koopmans T. About the assignment of wave functions and eigenvalues to the individual electrons of an atom. *Physica.* 1 (1934) 104–113.
61. Parr R.J, Pearson R.G. Absolute hardness: companion parameter to absolute electronegativity. *J. Am. Chem. Soc.* 105 (1983) 7512-7516.
62. A. A. El-Bindary, A. Z. El-Sonbati, M. A. Diab, and M. K. Abd El-Kader, Potentiometric and Thermodynamic Studies of Some Schiff-Base Derivatives of 4-Aminoantipyrine and Their Metal Complexes, *Journal of Chemistry*, 2013, Article ID 682186, 6 pages, 2013. <https://doi.org/10.1155/2013/682186>.

63. R. G. Pearson. Absolute electronegativity and hardness: applications to organic chemistry. *J. Org. Chem.* 54 (1989) 1423-1430.
64. Gurbel PA, Kuliopulos A, Tantry US. G-Protein–Coupled Receptors Signaling Pathways in New Antiplatelet Drug Development. *Arterioscler Thromb Vasc Biol.* 35 (2015) 500-512.
65. Parrales A, López E, López-Colomé AM. Thrombin activation of PI3K/PDK1/Akt signaling promotes cyclin D1 upregulation and RPE cell proliferation, *Biochimica et Biophysica Acta (BBA) - Molecular Cell Research*, 1813 (2011) 1758-1766.
66. Reema G, Polly J.P, Daniel M.R and Joseph J.B. α -Thrombin Induces Rapid and Sustained Akt Phosphorylation by β -Arrestin1-dependent and -independent Mechanisms, and Only the Sustained Akt Phosphorylation Is Essential for G1 Phase Progression*. *J Biol Chem*, 277 (2002) 18640-18648.
67. Toker A. Protein Kinases as Mediators of Phosphoinositide 3-Kinase Signaling. *Mol. Pharmacol.* 57 (2000) 652–658.
68. Ellis CA, Malik AB, Gilchrist A, Hamm H, Sandoval R, Voino-Yasenetskaya T, Tirupathi C. Thrombin induces proteinase-activated receptor-1 gene expression in endothelial cells via activation of Gi-linked Ras/mitogen-activated protein kinase pathway. *J Biol Chem.* 274 (1999) 13718-27
69. Cabrera-Vera TM, Vanhauwe J, Thomas TO, Medkova M, Preininger A, Mazzoni MR, Hamm HE. Insights into G protein structure, function, and regulation. *Endocr Rev.* 24 (2003) 765–781.
70. Wettschureck N, Offermanns S. Mammalian G proteins, and their cell type-specific functions. *Physiol Rev.* 85 (2005) 1159–1204.

GA



ACCEPTED MANUSCRIPT

Highlights

- Novel 2-cyclopropyl-3-ethynyl-4-(4-fluorophenyl) quinolines (**4a-1**) were recognized as GPCR ligands through molecular evaluations.
- Thrombin mediates adhesion of mast cell, a type of cell abundantly found in connective tissue and releasing histamine and other substances during inflammatory and allergic reactions, through phosphoinositol 3-kinase pathway.
- **4a-1** were able to bid on the binding pocket of PI3Kinase with low binding affinity
- Platelet aggregation and cytotoxicity assessment results revealed the druggability of **4a-1** as GPCR (PAR1) ligands.